The Dynamic Response of the Greenland and Antarctic Ice Sheets to Multiple-Century Climatic Warming

PHILIPPE HUYBRECHTS

Departement Geografie, Vrije Universiteit Brussel, Brussels, Belgium, and Alfred-Wegener-Institut für Polar- und Meeresforschung, Bremerhaven, Germany

JAN DE WOLDE

Instituut voor Marien en Atmosferisch Onderzoek, Universiteit Utrecht, Utrecht, Netherlands

(Manuscript received 7 January 1998, in final form 20 July 1998)

ABSTRACT

New calculations were performed to investigate the combined response of the Greenland and Antarctic ice sheets to a range of climatic warming scenarios over the next millennium. Use was made of fully dynamic 3D thermomechanic ice sheet models, which were coupled to a two-dimensional climate model. The experiments were initialized with simulations over the last two glacial cycles to estimate the present evolution and were subsequently forced with temperature scenarios resulting from greenhouse emission scenarios which assume equivalent CO_2 increases of two, four, and eight times the present (1990 A.D.) value by the year 2130 A.D. and a stabilization after that. The calculations brought to light that during the next century (short-term effect), the background evolution trend would dominate the response of the Antarctic ice sheet but would be negligible for the Greenland ice sheet. On that timescale, the Greenland and Antarctic ice sheets would roughly balance one another for the middle scenario (similar to the IPCC96 IS92a scenario), with respective contributions to the worldwide sea level stand on the order of about ± 10 cm. On the longer term, however, both ice sheets would contribute positively to the worldwide sea level stand and the most important effect would come from melting on the Greenland ice sheet. Sensitivity experiments highlighted the role of ice dynamics and the height–mass-balance feedback on the results. It was found that ice dynamics cannot be neglected for the Greenland ice sheet, not even on a century timescale, but becomes only important for Antarctica on the longer term. The latter is related to an increased outflow of ice into the ice shelves and to the grounding-line retreat of the west Antarctic ice sheet, which are both found to be sensitive to basal melting below ice shelves and the effective viscosity of the ice shelves. Stretching parameters to their limits yielded a combined maximum rate of sea level rise of 85 cm century^{-1}, of which 60 cm would originate from the Greenland ice sheet alone.

1. Introduction

There are increasingly convincing indications that the observed global warming of between 0.3° and 0.6°C over the last 100 yr bears the signature of human influence (Santer et al. 1995, 1996). With greenhouse gas concentrations anticipated to rise further, it is predicted that the anthropogenic effect will lead to an additional global climatic warming of between 1° and 3.5°C by the end of the next century, with the likelihood of a larger warming after that date if greenhouse gas emissions are not greatly reduced (Houghton et al. 1996). Calculations with GCMs indicate that this warming would be most pronounced in the polar latitudes, by up to a factor of 2–3 of the global average. A frequently mentioned aspect of such a climatic warming are changes in global sea level. On a decadal-to-century timescale, it is generally believed that the effects of thermal expansion and glacier melting will dominate the sea level response (e.g., Wigley 1995; de Wolde et al. 1997). On the longer term, however, by far the largest potential contribution is to be expected from the ice sheets of Antarctica and Greenland, which would, if melted entirely, contribute between 70 and 75 m to the worldwide sea level stand. Although the entire melting of these ice sheets can be ruled out to occur within the next few centuries, even with a sustained warming of up to 10°C (Letreguilly et al. 1991; Huybrechts 1994a), it is clear already that a few percent change in their volume would have wide-ranging implications for mankind.

The response of the Greenland and Antarctic ice sheets to future warming has been addressed in several modeling studies (Oerlemans 1982; Huybrechts and Oerlemans 1990; Huybrechts et al. 1991; Drewry and

Corresponding author address: Dr. Philippe Huybrechts, Department Geografie, Vrije Universiteit Brussel, Pleinlaan 2, B-1050 Brussel, Belgium.
E-mail: phuybrec@vub.ac.be

Morris 1992; Budd et al. 1994; Loutre 1995; Verbitsky and Oglesby 1995; van de Wal and Oerlemans 1997). These studies underlined the fundamentally different climatic and glaciological settings of both ice sheets, which is well characterized by a 10°–15°C temperature difference in the annual mean. Whereas the Antarctic ice sheet is presently surrounded by ice shelves and located in a region where little or no surface melting occurs, the Greenland ice sheet is situated in a region where temperatures are high enough to cause widespread summer melting. As a consequence, the Antarctic ice sheet is generally expected to grow in a warmer climate because the increased accumulation rates associated with a warming would dominate over increased melting rates. Warming over the Greenland ice sheet, on the other hand, would strongly enhance melting at the margin and hence lead to a shrinking ice sheet. However, much would also depend on the magnitude and duration of the warming, and on how mass-balance changes are related to temperature and precipitation changes.

In recent state-of-the-art assessments, it is found that for a realistic range of warming over the next hundred years, the Antarctic and Greenland contributions to sea level change would largely balance each other and be on the order of about ± 10 cm (IPCC second scientific assessment; Warrick et al. 1996; de Wolde et al. 1997). However, these estimates either ignore the dynamic response of the ice sheets or assume that the ice sheets are in equilibrium with the present climate. Neither of these assumptions is probably well justified. Nor does it indicate that both ice sheets would continue to show a counteracting effect beyond the twenty-first century, even when temperatures would stabilize at their 2100 A.D. values.

When discussing the role of ice dynamics, two aspects need to be considered. First, because of the long reaction timescales introduced by isostasy, thermomechanical coupling, and the advection of ice with different rheological properties in the basal shear layers, it seems unlikely that the ice sheets have adjusted completely to their past history. Even in the absence of any present-day climatic perturbations, the Antarctic and Greenland ice sheets are expected to respond to past changes of their surface boundary conditions for a long time to come, in particular to those changes associated with the last glacial–interglacial transition. In effect, the imbalance of polar ice sheets provides the major source of uncertainty to explain the observed mean global sea level rise of 18 cm over the last century, only half of which can be accounted for by the mean estimates for thermal expansion and melting of small glaciers over the same time interval (Warrick et al. 1996).

Second, it can be questioned whether it is really appropriate to study the response of ice sheets by integrating changes of the ice sheet mass balance forward in time without compensating for changes in ice sheet geometry (e.g., Wigley 1995; Raper et al. 1996). This is because a changing mass balance will significantly affect the distribution of ice thickness and surface slope. The resulting changes in driving stress will influence the ice flow and thus the shape of the ice sheet, and this can in turn be expected to feed back on the mass-balance components. In Antarctica, there is the additional effect of changes in ice discharge from the grounded ice sheet into the ice shelves, and the possibility of grounding-line migration. The latter directly affects the volume of grounded ice above floating, which is the relevant quantity controlling changes of sea level. A related aspect is the potential occurrence of unstable behavior in the west Antarctic ice sheet, with its buttressing ice shelves and bed so far below sea level, though the possibility of a rapid collapse is nowadays regarded as probably too dramatic (Warrick et al. 1996; Bentley 1997).

In this paper, we make an attempt to address these issues and concentrate on the response of the Greenland and Antarctic ice sheets on a multiple-century timescale up to the year 3000. In particular the processes giving rise to a dynamic response as compared to a static approach are analyzed in more detail. These experiments are performed with high-resolution 3D thermomechanic models of the entire ice sheet–ice–shelf–lithosphere system. These are driven by climatic output generated by a two-dimensional climate/ocean model subjected to greenhouse emission scenarios, which assume concentration stabilization at various levels by the middle of the twenty-second century. To distinguish between the long-term ''background'' evolution and the anthropogenically induced response, the experiments were initialized with output originating from ice sheet runs over the last two glacial–interglacial cycles. Using updated mass-balance parameterizations, refined ice-dynamic treatments and a nonuniform forcing, these results extend previous work reported in Huybrechts and Oerlemans (1990), Huybrechts et al. (1991), Huybrechts (1994b), and de Wolde et al. (1997).

2. The models

Here only a general outline of the model is given, and more details on the various formulations are presented in the appendixes. The entire model consists of four main components that, respectively, describe the ice sheet system, the solid earth, the surface climate, and the interface between the ice surface and the atmosphere (the mass-balance model).

Both the Greenland and Antarctic ice sheet models solve the fully coupled thermomechanical equations for ice flow on a high-resolution three-dimensional grid and include basal sliding and a temperature calculation within the bedrock. These models have a free interaction between climatic input and ice thickness, and are able to freely generate the ice sheet geometry in response to prescribed changes of sea level, surface temperature, and mass balance (snow accumulation minus ice ablation). A major distinction between the Greenland and

Antarctic ice sheet models is that the latter incorporates a coupled ice shelf model. Including ice shelf dynamics is required to enable interaction with the ocean and migration of the grounding line, which is the place separating the grounded from the floating ice domain. These models are described in more detail in appendix A and in Huybrechts (1990, 1996) and Huybrechts et al. (1991).

The bedrock model describes the interaction between changes in the ice loading and the bed elevation. A two-layer isostasy model is employed. The time-dependent response of the bed depression is given by the viscous properties of the asthenosphere, which is overlaid by a rigid elastic lithosphere that determines the ultimate shape of the imprint. The deformation of the earth's crust is basically driven by the density contrast between ice and mantle rock. More details on the way that bedrock adjustments are treated are presented in appendix B.

The third component of the model is the mass balance, which represents the link between the ice sheet and the climate system (atmosphere and ocean). The mass-balance model distinguishes between the snowfall rate on the one hand and meltwater runoff on the other hand. Both are parameterized in terms of temperature. Lacking a convincing alternative, the precipitation rate is based on its present distribution and perturbed in different climates according to sensitivities derived from ice-core studies. This means that only the precipitation intensity can change, and that the effects of changes in atmospheric circulation and orography are not included, but an alternative is hardly available. Present-day GCMs are not very good in their predicted patterns of precipitation and precipitation change and moreover show little resemblance among themselves. An exception seems to be the ECHAM3 model at a T106 resolution (Ohmura et al. 1996), but those results are only available for short time periods because of computer limitations. The snowfall rate, which is the relevant parameter for the mass balance, is in the model a fraction of the precipitation rate depending on the surface temperature. As long as the ice sheet does not drastically change its dimensions, the assumption of a stationary precipitation pattern is probably the best one can do. It at least ensures that the present state is represented in the best possible way.

The melt-and-run-off model is based on the degree–day method and is similar to the model described in Reeh (1991). Although the annual melt rate depends on the details of the energy balance at the ice sheet surface, it is not feasible to perform a full energy balance calculation for all ice sheet points at all times. Moreover, van de Wal (1996) has shown that within the range of uncertainty of crucial parameters, the degree–day method and the energy balance method yield very similar results. The melt-and-runoff model further takes into account ice and snow melt, the daily temperature cycle, random temperature fluctuations around the daily mean, liquid precipitation, and refreezing of meltwater (appendix C).

The mass-balance model is driven by prescribed temperature changes. These arise from a coupled climate and ocean model, which is driven by prescribed equivalent CO_2 concentrations as a function of time. The climate model used for this purpose is a two-dimensional energy balance model, having latitudinal and seasonal resolution (Bintanja 1997). The surface air temperature results from radiative fluxes at the surface and at the top of the atmosphere, from turbulent fluxes between the atmosphere and surface, from latitudinal heat transport, and from the calculated snow cover. It is coupled to an ocean model, which consists of three zonally averaged basins, representing the Atlantic, Pacific, and Indian Oceans, and which are connected by a circumpolar ocean basin, representing the Southern Ocean. The ocean temperature field is affected by ocean heat mixing, by advection by the mean flow, and by heat exchange at the surface. This coupled climate and ocean model was used in one of the sets of the IPCC96 sea level projections (Warrick et al. 1996; de Wolde et al. 1997) and is described in more detail in appendix D. Using similar forcings, the temperature results were compared to several coupled GCM results and found to be in good agreement (de Wolde 1996). Resulting changes of the ice sheet geometries are too small in most of the experiments to have a significant influence on the climatic input. Therefore, the feedback of ice sheet changes on the temperature perturbations produced by the climate model are not taken into account.

3. Experimental setup

All results are obtained for a time window stretching from 1990 to 3000, with the year 1990 taken as the reference state to which results are compared. Instead of defining a reference state that is in equilibrium with present-day boundary conditions, as has been done in previous studies, we specifically opted to deal with the inertial effects associated with the various components of the ice sheet–climate system. That makes it necessary to start the calculations at an earlier time. All models were subsequently tuned within the error limits of crucial parameters to reproduce the present state of the ice sheets close to the initial data (Table 1).

a. The present evolution of the ice sheets

Ice sheets and their underlying bedrock have the longest response timescales, which are on the order of 10^2 to 10^4 yr. Therefore, the ice sheet and bedrock models were first initialized with calculations over the last two glacial cycles. As initial conditions during the one-but-last interglacial served output from a similar glacial cycle run at the present time, so that in total four glacial cycles were calculated. Such a period is more than sufficient for the models to forget their start-up conditions. It was assumed that the observed present-day bedrock was in isostatic equilibrium with the observed present-

TABLE 1. Modeled geometric characteristics of the Greenland and Antarctic ice sheets for the present time compared with the input data (Huybrechts 1992, 1996). All data use a constant grid-cell area on a polar stereographic projection with standard parallel at 71° latitude and have not been corrected for distortions caused by the map projection. Modeled and observed data are within 5%–10%, which is well within the range of uncertainty on the measured values.

	Area (10^6 km^2)	Volume (10^6 km^3)	Mean ice thickness (m)	Maximum surface elevation (m)
Greenland, glacial cycle at present	1.7880	3.0519	1706.8	3256.4
Greenland, input model data	1.6708	2.8249	1690.7	3246.3
Antarctica, glacial cycle at present	12.5920	26.3719	2094.3	4087.1
Antarctica, input model data	12.6960	25.0214	1970.8	4023.1

day ice and water loading. The latter may not be entirely the case but does not have much influence on the rate of change for the present day, which is of main interest. The temperature and accumulation forcings in these runs were, respectively, derived from the Greenland Ice-core Project ice core (Dansgaard et al. 1993) and the Vostok ice core records (Jouzel et al. 1993). The sea level history was derived from the spectral mapping (SPECMAP) group at Brown University stack (Imbrie et al. 1984). The imbalance of the ice sheet is then defined by the thickness change at the present time. A calculation of this type provides an alternative over classic geodetic, remote sensing, or mass-balance techniques, which are unable to constrain the imbalance to better than $\pm 25\%$ (Warrick et al. 1996). The quality of such a calculation depends on how good past climatic conditions can be described and on how good the ice sheet models deal with dynamic aspects (such as ice-temperature evolution, flow law, grounding-line migration, etc.).

The results of these simulations have been compared against available geological and glaciological (palaeo-) field evidence and were shown to be in reasonably good agreement (Huybrechts 1992; van Tatenhove et al. 1995). In particular the retreat history of the ice sheet in central west Greenland is well constrained by field data. The retreat of the west Antarctic ice sheet, on the other hand, cannot be unambiguously confirmed by independent field evidence and takes place in the model between 9000 and 4000 calendar years before present. This timing coincides with the ICE-3G chronology derived from relative sea level data by Tushingham and Peltier (1991), but other chronologies indicating an earlier retreat between 12 000 and 6000 years ago have also been proposed (e.g., Nakada and Lambeck 1988; Denton et al. 1990)

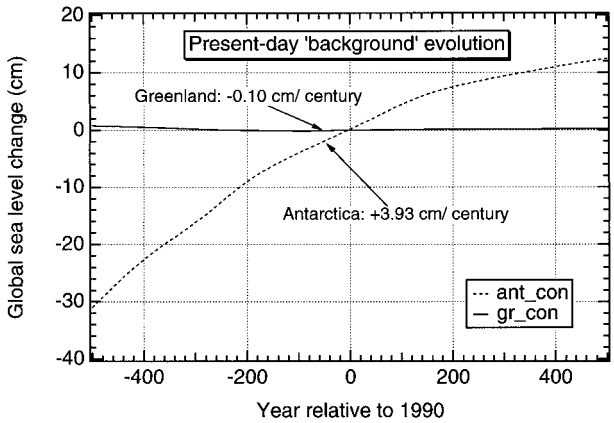

FIG. 1. The background evolution of the Greenland and Antarctic ice sheets resulting from simulations over the last two glacial–interglacial cycles. The past climatic forcing is taken from ice-core and oceanic sediment records and kept constant after the year 1990.

Figure 1 displays the outcome of these simulations in a window comprising the last 500 yr and extending up to 500 yr after present. In these graphs, ice volume changes were transformed into global sea level changes by assuming a constant oceanic surface area of 3.62×10^8 km^2. It turns out that the Greenland ice sheet is near to stationary with only a small growing trend, corresponding to a global sea level lowering over the last 100 yr of around 0.10 cm only. This value is slightly lower than the 0.35 cm century^{-1} of sea level lowering reported in Huybrechts (1994b), which is due to a slightly different forcing (GRIP vs a combined temperature record from the Dye3 and Camp Century ice cores), but the basic result is confirmed. The Antarctic ice sheet, on the other hand, is found to be still reacting to grounding-line retreat in west Antarctica following the last glacial–interglacial transition. In terms of sea level variations, the results indicate an imbalance equal to a global sea level rise of $+0.39$ mm yr^{-1} averaged over the last 100 yr. Interestingly, Antarctica alone accounts for a significant part of the unexplained sea level rise over the last century (Warrick et al. 1996). Up to the year 3000, the trend under constant climate forcing would produce a global sea level rise of 17.8 cm resulting from the Antarctic ice sheet and of only 0.49 cm due to changes of the Greenland ice sheet. Nevertheless, error bands remain substantial. This is particularly true for the Antarctic ice sheet, where small phase shifts in the forcing have a significant effect on the model outcome.

b. The temperature forcing in the future

To derive climatic scenarios for the future, the climate model was first calibrated against the seasonal cycle of present-day observations of surface air temperature, ocean temperature, and snow and sea-ice cover. Then a preindustrial model state was obtained by means of the

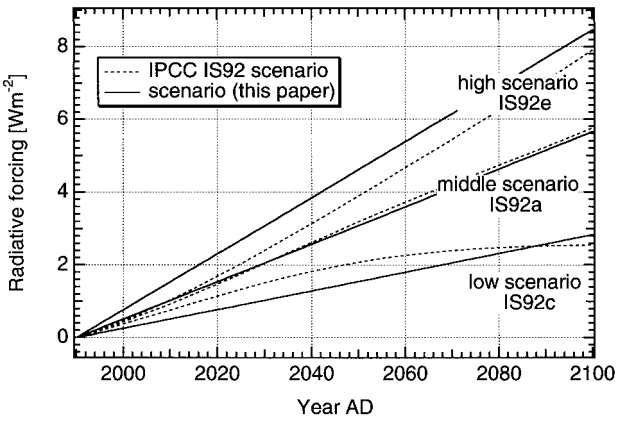

FIG. 2. Radiative forcing derived for the low ($2 \times CO_2$), middle ($4 \times CO_2$), and high ($8 \times CO_2$) scenarios of this study as compared to the IPCC96 IS92a, IS92e, and IS92c scenarios with constant aerosol concentrations at the 1990 level.

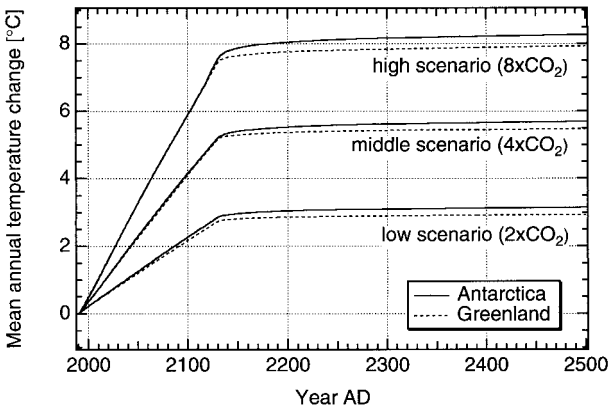

FIG. 3. Mean annual temperature rise predicted by the two-dimensional climate and ocean model for the three scenarios tested in this paper. Values are averaged over the entire Greenland and Antarctic model grids. Equivalent CO_2 concentrations rise until 2130 A.D. and are kept constant after that.

historical (1765) radiative forcing value. In order to deal with the effects originating from the thermal inertia of the oceans, and to circumvent the so-called cold-start problem (Hasselmann et al. 1993), model scenario calculations then start from this preindustrial model state, following the observed historical radiative forcing values (Kattenberg et al. 1996) from 1765 to 1990.

We then prescribed three different scenarios of equivalent CO_2 concentration increases that approximately matched the IPCC96 constant-aerosol radiative forcing scenarios IS92c, IS92a, and IS92e until the year 2100 (Fig. 2). This could conveniently be done by prescribing equivalent CO_2 increases of 0.5%, 1%, and 1.5% per year, and transforming these in a radiative forcing using a sensitivity of 5.17 W m^{-2} (Bintanja 1997) for every *e*-fold increase in CO_2 concentration. These relations were extrapolated for another 30 years until 2130 to yield a radiative forcing of, respectively, +3.61, +7.16, and +10.75 W m^{-2} above the level of 1990, which is equivalent to the effect of two, four, and eight times the present CO_2 concentration. When using the slightly different sensitivity value of 6.3 W m^{-2} adopted for the IPCC96 assessment (Kattenberg et al. 1996), these final radiative forcings would, respectively, correspond to 608, 1068, and 1888 ppmv equivalent CO_2, that is, 2.2, 3.8, and 6.8 times the preindustrial CO_2 concentration of 278 ppmv.

After the year 2130 and up to the year 3000, we opted for concentration stabilization at the 2130 level, simply because there are little concrete starting points to prefer one emission reduction scenario above another. Obviously, other emission scenarios would yield a different temperature response and hence lead to different predictions of global sea level change, but the three scenarios established here are believed to cover a realistic bandwidth of temperature changes for a wide range of possible emission scenarios (Walker and Kasting 1992; Kim and Crowley 1994; Wigley 1995) and moreover provide an acceptable range of boundary conditions to investigate the dynamic response of the Antarctic and Greenland ice sheet during the next thousand years.

The mean annual temperature evolution over both the Antarctic and Greenland ice sheets is displayed in Fig. 3. It shows the typical transient response to a ''ramp'' forcing, exhibiting nearly linear temperature increases up to 2130 A.D., followed by a slow warming after that due to the delayed response of the ocean. Such behavior is very similar to GCMs subjected to a comparable forcing (e.g., Manabe and Stouffer 1993). The ensuing latitudinal and seasonal temperature changes in the year 3000 for the middle scenario are presented in Fig. 4, showing how the warming is largest near to the poles and during the winter. That is also in agreement with most GCM results.

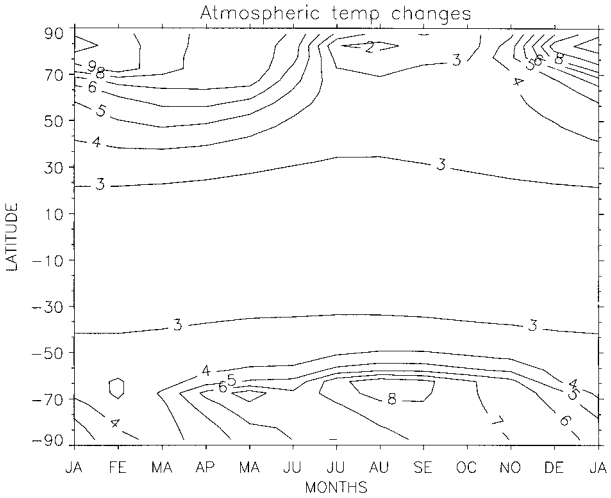

FIG. 4. Global atmospheric temperature changes from the coupled climate and ocean model at the end of the simulation in the year 3000 A.D. Temperature changes are displayed as perturbations with respect to 1990 A.D. for the middle scenario ($4 \times CO_2$).

TABLE 2. Overview of model runs involving the Greenland ice sheet. All global sea level results are given with respect to 1990 A.D.

Experiment	Scenario	Response	Background trend included	Global sea level change at 2130 A.D. (cm)	Global sea level change at 3000 A.D. (cm)
gr_con	Control	Dynamic	Yes	+0.1	+0.5
gr_low	Low	Dynamic	Yes	+6.8	+87.5
gr_mid	Middle	Dynamic	Yes	+20.3	+316.7
gr_high	High	Dynamic	Yes	+41.1	+578.1
gr_dyn	Middle	Dynamic	No	+20.2	+316.2
gr_stat	Middle	Static	No	+25.6	+233.6
gr_fix	Middle	Fixed geometry	No	+21.2	+154.3

4. Future ice sheet changes

To facilitate interpretation of the results, an overview of the experiments, with a brief description of their differences and their main result, is presented in Tables 2 and 3.

a. Projected contributions to global sea level

Figure 5 shows the projected sea level changes of both ice sheets for the three scenarios up to the year 2100 A.D. By 2130 A.D., when greenhouse gas concentrations stabilize at, respectively, two (low), four (mid), and eight times (high) their present values, the projections for Greenland range between 6.8 cm (gr_low) and 41.1 cm (gr_high), with a ''best'' projection of 20.3 cm (gr_mid), whose values are almost twice as much of those shown for 2100 A.D. in Fig. 5. The background evolution (gr_con) during this time interval is negligible compared to the climatic change runs, so that the assumption of stationarity seems to be justified for the Greenland ice sheet. For the Antarctic ice sheet, on the other hand, the situation is entirely different. Here, the response is dominated by the background trend until at least the end of the twenty-first century. Only after that date a growing trend, resulting in a sea level fall, becomes evident. Sea level contributions by the year 2130 are, respectively, +6.0 cm (background trend), and between −0.6 cm (ant_low), −6.4 cm (ant_mid), and −11.1 cm (ant_high) for the perturbed runs.

Interestingly, both ice sheets balance one another up to the second half of the twenty-first century, but only as far as their behavior relative to the background trend is concerned. For instance, by the year 2100 in the middle scenario (identical to the IPCC IS92a scenario; Houghton et al. 1996), the Greenland ice sheet would contribute +10.6 cm to the global sea level stand and the Antarctic ice sheet −8.1 cm (relative to the background trend), but in the high scenario these numbers have already diverged to +21.2 and −11.6 cm, respectively. Beyond the next century, or after taking into account the predicted imbalance for the Antarctic ice sheet, this approximate balance no longer holds, and the Greenland ice sheet clearly dominates the response, in spite of the fact that it contains about eight times less ice than the Antarctic ice sheet. That is because changes in Greenland's mass balance are dominated by melting, which has a much larger sensitivity to temperature change than precipitation.

TABLE 3. Overview of model runs involving the Antarctic ice sheet. Here τ^* is the characteristic response timescale for ice shelf temperature change used in the flow law; $\tau = 0$ indicates that the effective ice shelf temperature instantaneously follows the surface perturbation; $\tau = \infty$ indicates that the effective ice shelf temperature remains fixed throughout the experiment. S is the basal melting rate below the fringing ice shelves. Global sea level results are given with respect to 1990 A.D. See main text for more details on the various experimental setups.

Experiment	Scenario	Response	Background trend included	τ^* (yr)	S (m yr^{-1})	Global sea level change at 2130 A.D. (cm)	Global sea level change at 3000 A.D. (cm)
ant_con	Control	Dynamic	Yes	500	0	+6.0	+17.8
ant_low	Low	Dynamic	Yes	500	0	−0.6	−32.1
ant_mid	Middle	Dynamic	Yes	500	0	−6.4	−62.2
ant_high	High	Dynamic	Yes	500	0	−11.1	+78.6
ant_dyn	Middle	Dynamic	No	500	0	−12.4	−80.0
ant_stat	Middle	Static	No	500	0	−13.8	−181.8
ant_fix	Middle	Fixed geometry	No	500	0	−13.9	−200.1
ant_tzero	Middle	Dynamic	No	0	0	−6.9	+117.9
ant_tinf	Middle	Dynamic	No	∞	0	−12.7	−114.1
ant_s1	Middle	Dynamic	No	500	1	−10.8	+30.0
ant_s3	Middle	Dynamic	No	500	3	−8.0	+107.1
ant_s5	Middle	Dynamic	No	500	5	−4.5	+168.4
ant_s10	Middle	Dynamic	No	500	10	+2.3	+176.4

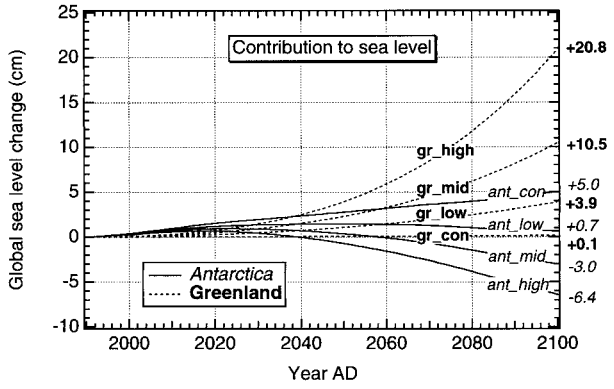

FIG. 5. Short-term response of the Greenland and Antarctic ice sheets to climatic warming up to the year 2100 A.D. Ice volume changes were transformed into global sea level changes assuming an ice density of 910 kg m^{-3} and a constant oceanic surface area of 3.62 $\times$ 10^8 km^2, or 71% of the earth's surface. Bold text refers to Greenland, italic text to Antarctica.

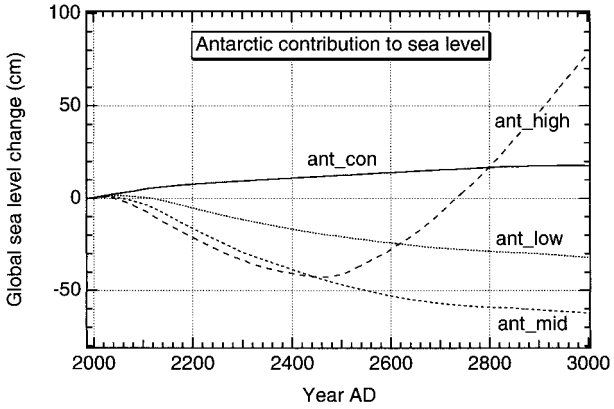

FIG. 7. Longer-term response of the Antarctic ice sheet to three climatic warming scenarios (low, 2 $\times$ CO_2; mid, 4 $\times$ CO_2; high, 8 $\times$ CO_2) up to the year 3000 A.D. expressed in equivalent changes of global sea level. In these experiments, the background evolution (ant_con) is retained as a contribution.

Although the predicted warming approximately stabilizes after the middle of the twenty-second century, that is not at all the case for the ice sheet's response, which continues to react to the imposed climatic change. For the Greenland ice sheet (Fig. 6), this occurs at an almost constant rate of between 9 cm $century^{-1}$ (gr_low) to up to 60 cm $century^{-1}$ (gr_high) of global sea level equivalent. In the latter case, the Greenland ice sheet has lost about three-quarters of its volume and has shrunk to 30% of its present-day area.

The behavior of the Antarctic ice sheet is much more complicated (Fig. 7). For temperature rises below about 6°C (low and middle scenarios), the ice sheet displays a small but continuous growing trend that produces a global sea level fall of between 30 and 50 cm by the end of the next millennium, that is, an order of magnitude smaller than the response of the Greenland ice sheet, but of opposite sign. The response to the high scenario, on the other hand, at first displays a growing ice sheet, but this is reversed after the year 2400. As shown in Fig. 8, this reversing trend is due to the onset of significant grounding-line migration, which is only minimal in the middle and low scenarios. The corresponding loss of grounded ice by the year 3000 in the high scenario involves a surface area of about 3.25 $\times$ 10^5 km^2, or about 2.5% of the total grounded area of the present ice sheet. A further analysis indicates that this grounding-line retreat is due both to increased surface melting in the marginal zone and to the effect of a warming ice shelf. The latter causes the ice shelf to deform more easily, which leads to larger flow velocities and a thinning. Grounding-line retreat follows when the thinning propagates across the grounding line and hydrostatic equilibrium needs to be restored.

A comparison of these results (Huybrechts and Oerlemans 1990; Huybrechts et al. 1991) with older versions of the mass-balance and ice sheet models display

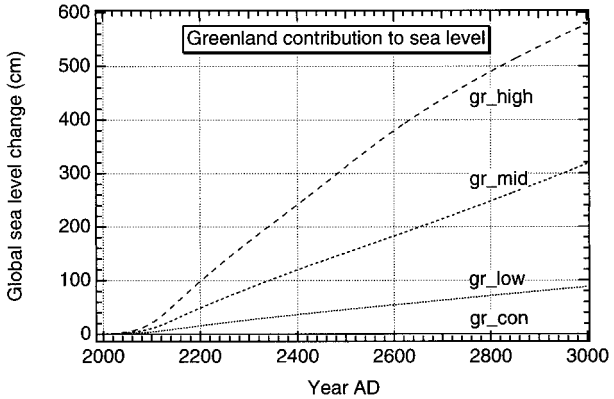

FIG. 6. Longer-term response of the Greenland ice sheet to three climatic warming scenarios (low, 2 $\times$ CO_2; mid, 4 $\times$ CO_2; high, 8 $\times$ CO_2) up to the year 3000 A.D. expressed in equivalent changes of global sea level. In these experiments, the background evolution (gr_con) is retained as a contribution.

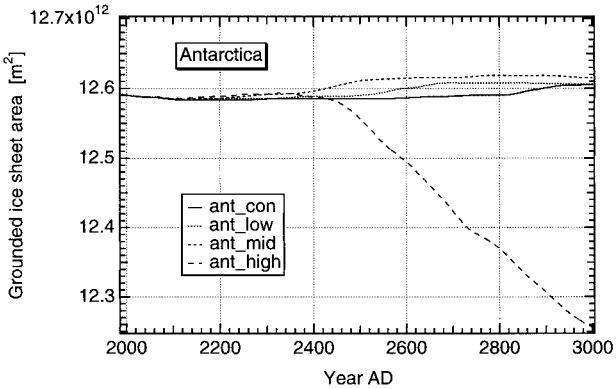

FIG. 8. Change of the grounded ice area of the Antarctic ice sheet for the experiments shown in Fig. 7. Details of the experimental setup are listed in Table 3. Except for the high scenario, grounding-line migration is very limited.

some differences, especially for the high scenario. On the one hand, the Greenland ice sheet melts more quickly. That can be explained by the higher sensitivity of the mass-balance treatment adopted in this paper for warmer climates. A distinction is made here between rainfall and snowfall, and the formation of superimposed ice now depends on temperature. For mean monthly temperatures above +2°C, more than half of the precipitation is now modeled to occur as rainfall, which will increasingly run off as the parameterization does not allow for the production of superimposed ice for mean annual temperatures above the freezing point. An important change in the Antarctic ice sheet model, on the other hand, concerns the treatment of the effective viscosity of the ice shelf, which depends on the temperature of the ice. In the 1990 paper, viscosity changes immediately followed surface temperature. In this work, a characteristic time lag of $\tau^* = 500$ yr was introduced (cf. appendix A), which makes the ice shelf thin less rapidly and leads to less grounding-line retreat.

b. The importance of surface melting

The role of surface melting in the evolution of both ice sheets is demonstrated in Fig. 9, showing the ratio of mean ablation rate relative to the mean accumulation rate. A ratio of 100 means that the amount of snowfall that accumulates on the ice sheet's surface runs off at the margin. Such an ice sheet can only exist in steady state provided there is no calving. For a ratio higher than 100, the ice sheet must shrink until the balance between accumulation on the one hand and runoff and calving on the other hand can be restored, for instance, by modification of its height–elevation distribution. For a ratio less than 100, the stability of the ice sheet will depend on the amount of calving. As shown in Fig. 9a (Greenland ice sheet), there is at present a roughly 50%–50% ratio between runoff and calving (assuming a balanced mass budget, which the background evolution suggests). Only in the low scenario does the ice sheet tend to a new stationary state, involving a smaller ice sheet with a higher height-to-width ratio. In the middle and high scenarios, however, melting is far too strong to be countered by increased accumulation and the Greenland ice sheet is irreversibly melting down on a timescale on the order of a few thousand years. The upper curve (gr_high) shows how the height–mass-balance feedback becomes active after 2300 A.D. That is because a melting ice sheet produces lower surface elevations, which in turn enhances the melting.

On Antarctica (Fig. 9b), surface runoff is insignificant (<5%) for the low and middle scenarios. As these scenarios involve little grounding-line migration (Fig. 8), the bulk of the response must be due to the effect of the increased accumulation rates as superimposed on the background trend. Runoff becomes more significant in the high scenario, however. As the melting is confined to the low-lying coastal areas, this also leads to some grounding-line migration.

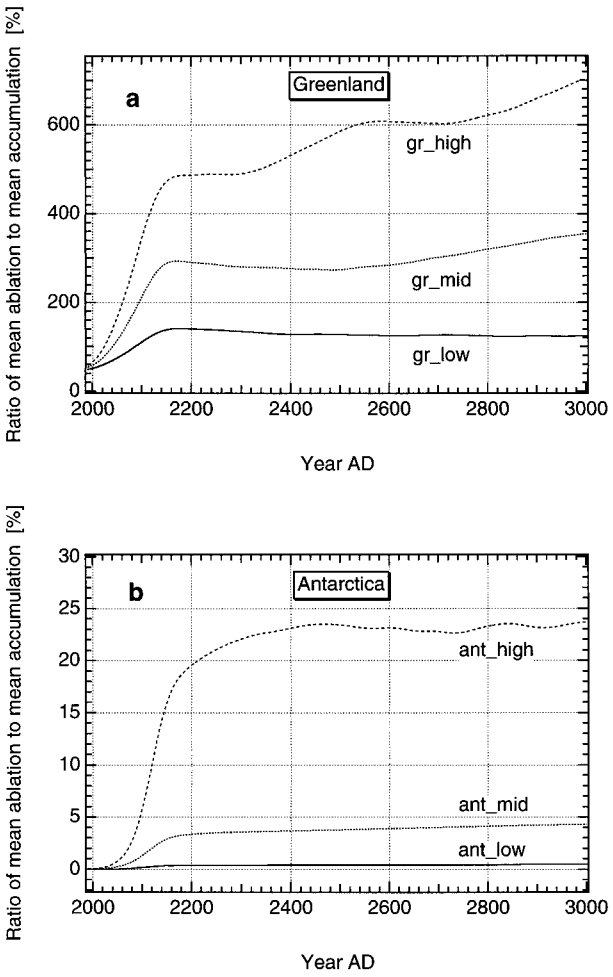

FIG. 9. Ratio of mean ablation to mean accumulation over the Greenland ice sheet (a) and the Antarctic ice sheet (b) for the various warming scenarios discussed in the paper (low, 2 × CO_2; mid, 4 × CO_2; high, 8 × CO_2).

The fundamental difference between the behavior of the Greenland and Antarctic ice sheets is due to how surface mass balance varies with temperature. On the Antarctic ice sheet, the increase in accumulation rates is able to outweigh the increase in runoff for temperature rises below about 5°C (Huybrechts and Oerlemans 1990), which in absolute terms then represents less than 10% of the total accumulation. Runoff balances accumulation only for temperatures more than 11°C above present levels. The Greenland ice sheet, on the other hand, today already experiences important summer melting. Here, runoff would exceed accumulation for a temperature rise of only 2.7°C (Huybrechts et al. 1991).

5. The role of ice dynamics

To better investigate the role of ice dynamics in the ice sheet's response, three different experimental setups

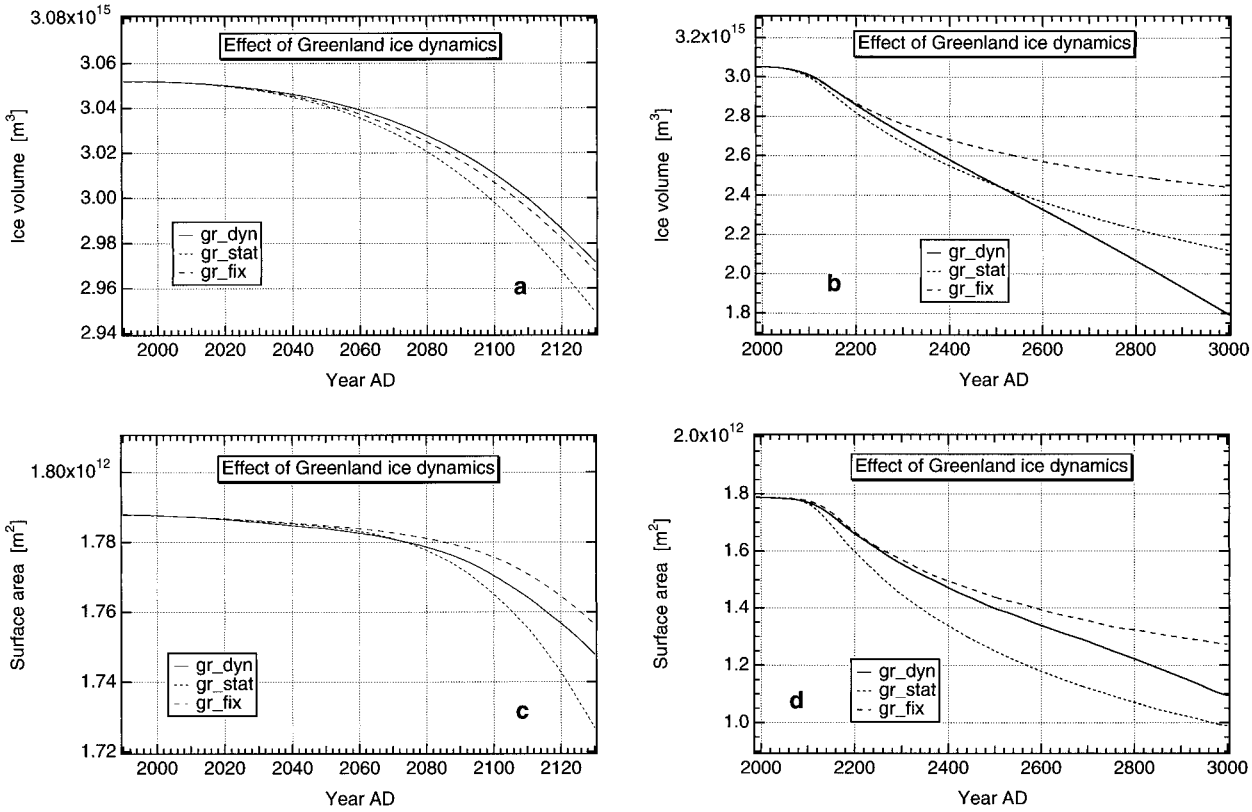

FIG. 10. Evolution of key variables in a series of experiments testing the role of ice dynamics. Shown are (a), (b) ice volume and (c), (d) surface area, (a), (c) both on the short term until 2130 A.D.; and (b), (d) as up to the end of the next millennium. Details of the experiments are given in Table 2 and in the text (gr_dyn, dynamic response; gr_stat, static response; gr_fix, fixed-geometry response).

are defined. A distinction is made between a static, a dynamic, and a fixed-geometry response.

The *dynamic response* is the one discussed so far in which there is a full coupling between the climatic perturbation, the mass balance, the ice thickness, and the stress distribution. The ice flow is in this case allowed to react to changes in the specific balance, the bedrock response, and the driving stress (ice thickness and surface slope).

In the *static response,* changes in ice flow and bedrock response are excluded. In effect, the local flux divergence (flow pattern), and for Antarctica also the grounding line, are kept constant, but changes in ice thickness can still feed back on the mass balance.

For the *fixed-geometry response*, the ice sheet geometry is kept entirely constant, and only perturbations with respect to the present mass balance are integrated forward in time. In this case, the additional warming resulting from a lowering of the surface in the ablation zone is thus excluded.

The maximum amount of ice that can melt away is limited by the available ice thickness in all three cases. Comparing the dynamic with the static run isolates the role of ice dynamics proper, while a comparison between the static and fixed-geometry runs provides information on the strength of the elevation–mass balance feedback. All runs (dynamic, static, fixed geometry) are considered relative to the background evolution resulting from past changes in boundary conditions.

a. The Greenland ice sheet

Results for the Greenland ice sheet are displayed in Fig. 10. These are for the middle warming scenario (4 $\times$ CO_2), but the behavior is qualitatively similar for the other scenarios. Clearly, the various experimental setups lead to large differences. After a 1000-yr integration (Figs. 10b, d), there is a factor of 2 difference in the change of ice volume depending on how the ice sheet is allowed to interact with a changing surface mass balance. The inclusion of ice dynamics at first leads to a counteracting effect that makes the ice sheet shrink less rapidly. As shown in Figs. 10a and 10c, this is evident already from the beginning of the integration. Compared with the static run, the change of ice volume is reduced by 10% at 2015 A.D., by 20% at 2050, and by 24% at the year 2100, when it reaches a maximum. This counteracting effect can be explained by a dynamic thickening of the ablation area.

Two mechanisms appear to be responsible for the dynamic effect: the first is that surface slopes at the margin are steepened in response to increased balance

gradients. These can only be matched by larger ice fluxes across the equilibrium line and thus induce an increased transfer of ice mass into the melting zone, which leads to a thickening. The second mechanism involves a lower calving flux, as the velocity near to the margin, which depends on ice thickness to the fourth power (shear stress), is reduced because of the thinning and thus leads to less outflow of ice toward the ocean. Both mechanisms thus cause a higher surface level of the ablation zone, and consequently to less melting than would be the case when ice dynamics was not included.

After the twenty-first century, the counteracting effect introduced by ice dynamics gradually weakens and even changes sign after the year 2500 A.D. An explanation can be found by closer inspection of the evolution curves for surface area (Figs. 10c, d). Unlike the curves for ice volume, the curves for surface area do not show a dynamic effect that becomes stronger than the static effect after the year 2500 A.D. In Figs. 10c, d, the ice sheet domain in the static case is seen to shrink consistently more rapidly than the dynamic case by between 20% and 30% all along the integration. The mean thickness of the ice sheet is given by total volume divided by total surface area. It appears that the reversal of the counteracting effect in the volume response is coincident with a break in the evolution of mean ice thickness, which is found to increase until the year 2500 in line with a steepening of the surface slopes, but decreases quickly after that date. This suggests that ice dynamics causes a thinning of the central areas of the ice sheet after several centuries, which increasingly makes the ice sheet more vulnerable to the imposed warming.

Comparing the static run (gr_stat) with the fixed-geometry run (gr_fix), on the other hand, brings to light the equally important role played by the height–mass-balance feedback. This feedback arises because a lowering surface in the ablation zone creates a warmer surface climate and thus more melting. This is a positive feedback and is found to significantly speed up the wastage of the ice sheet and thus competes with the dynamic effect as described above. From Fig. 10, it can be seen that both effects roughly balance each other until the middle of the twenty-third century, but that after that date, the height–mass-balance effect must either become stronger and/or the counteracting effect introduced by ice dynamics must become weaker.

Apparently, neither ice dynamics nor the height–mass-balance feedback can be ignored when investigating the response of the Greenland ice sheet to future warming, and this not even on a century timescale.

Snapshots of the resulting ice sheet topographies in several runs are presented in Fig. 11. These show that margin retreat occurs most readily in the dry north and northeastern parts of the Greenland ice sheet and is followed later at the western side of the ice sheet. One of the implications is that in a warming climate calving in those parts must cease quickly and that ice wastage is taken over by meltwater runoff only. According to the simulations, calving glaciers are likely to survive the longest in the southeastern part of the Greenland ice sheet, where climatic conditions are at their wettest and equilibrium lines at their lowest. There, the ice sheet continues to extend down to sea level, even in the high scenario at the year 3000. One of the weakest points of the Greenland ice sheet then appears to be the saddle connecting the southern dome with the main ice sheet and that is also the place where the ice sheet separates into two smaller ice masses. The elevation of the central dome, on the other hand, is not much affected by marginal retreat and moreover does not seem to migrate much during decay of the Greenland ice sheet.

b. The Antarctic ice sheet

Because of its different climatological and glaciological setting, a parallel study on the Antarctic ice sheet provides an interesting contrast with the mechanisms described above. On the Antarctic ice sheet, surface melting is of minor importance and changes in the ice sheet configuration are primarily caused by grounding-line movements resulting from ice sheet–ice shelf interactions.

1) THE EFFECT OF ICE DYNAMICS IN THE STANDARD RUN

As shown in Fig. 12a, the incorporation of ice dynamics produces a clear counteracting effect, which progressively becomes stronger in time, causing the Antarctic ice sheet to contribute 6.3% less to the global sea level lowering by the year 2100 than would result from the direct mass-balance effect alone (static effect). This figure gradually rises to 30.8% by 2500 A.D. and to 56% at the end of the integration (3000 A.D.). As can be seen in Fig. 12b, this dynamic effect cannot be due to grounding-line migration, because there is hardly any change in the grounded ice sheet area (the total range involves only 18 gridpoints or 0.2% of the total area). Moreover, if anything, there is a seaward migration of the grounding line (mainly in the Ross and Ronne-Filchner ice shelves in response to the local thickening of some tens of meters), and this would produce an effect of opposite sign. Nor is there any significant runoff (Fig. 9b). A careful analysis revealed that the dynamic effect (after correcting for the background trend) causes the growth of grounded ice volume to slow down mainly because of an increase of the ice flux across the grounding line, which thus, in part, counteracts the thickening effect due to the increased accumulation rates. This increase of the flux across the grounding line is a result of both the local thickening at low elevations near to the grounding line, producing higher-shear stresses, and of an increased ice-mass discharge on the ice shelves that pulls the ice out of the grounded ice sheet and is effective a few grid points inland. This behavior reflects the comparably short response timescales near to the grounding

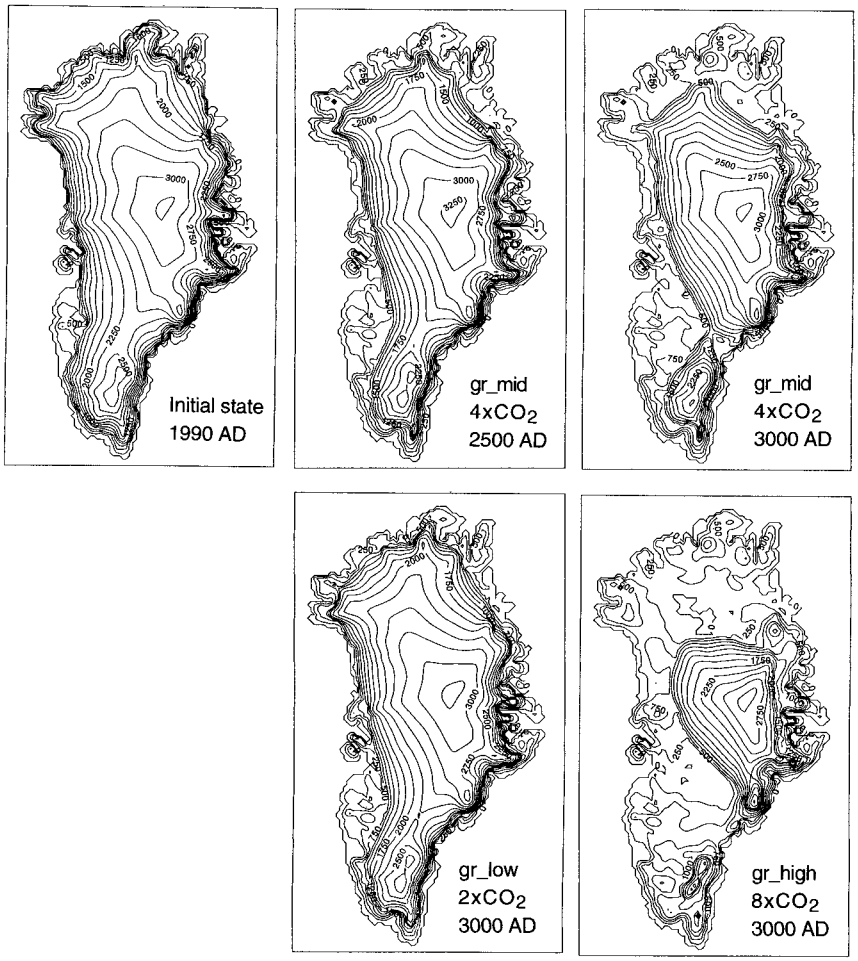

FIG. 11. Snapshots of Greenland surface elevation for the experiments and times indicated in the lower-right corner and further detailed in Table 2 and the main text. The ice sheet margin is easily distinguished by its high surface slope. Contour interval is 250 m.

line and in the ice shelf as compared to the bulk of the grounded ice sheet.

Comparing the static run (ant_stat) with the fixed-geometry (ant_fix) run in Fig. 12a brings to light that the height–mass-balance feedback is only of minor importance. This feedback reduces the growth of the ice sheet somewhat, basically because a thickening over the plateau leads to a lower mass balance. Nevertheless, the effect is very small and amounts to only 0.6% by the year 2100, 4.9% at 2500 A.D., and 9.1% at the end of the integration (3000A.D.) That is because of the very low accumulation rates and the absence of significant melting.

Also here, it appears that changes on the Antarctic ice sheet cannot be properly studied without taking into account ice dynamics, but in contrast to the Greenland ice sheet, the dynamic effect can be neglected on a century timescale and the height–mass-balance effect hardly plays a role.

2) THE EFFECT OF ICE SHELF TEMPERATURE

With most of the dynamic effect originating in the ice shelves, it is appropriate to concentrate in more detail on factors controlling its behavior, which were so far excluded from the analysis. A first factor concerns the treatment of the ice shelf temperature, which controls its effective viscosity. Warmer ice causes the ice shelf to deform more rapidly, leading to larger strain rates and a thinning. Transmission of these features across the grounding line will force the outflow from the grounded ice sheet to increase (because of larger shear stresses and longitudinal stress gradients) and will eventually lead to grounding-line retreat. In the standard run (ant_dyn), it was assumed that the ''effective'' deformation temperature of the ice shelf follows changes in the surface temperature with a characteristic time lag of 500 yr.

The effect of either excluding ice shelf warming (ant_tinf, $\tau^* = \infty$) or of an ice shelf that reacts instan-

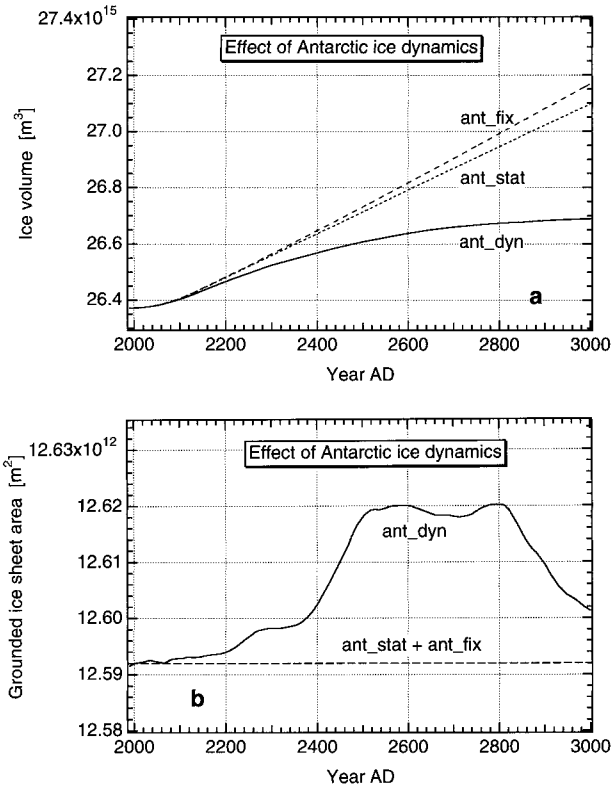

FIG. 12. Evolution of Antarctic ice volume (a) and grounded ice sheet area (b) in a series of experiments testing the role of ice dynamics. To enable a better comparison, all results are shown relative to the background trend (ant_dyn, dynamic response; ant_stat, static response; ant_fix, fixed-geometry response).

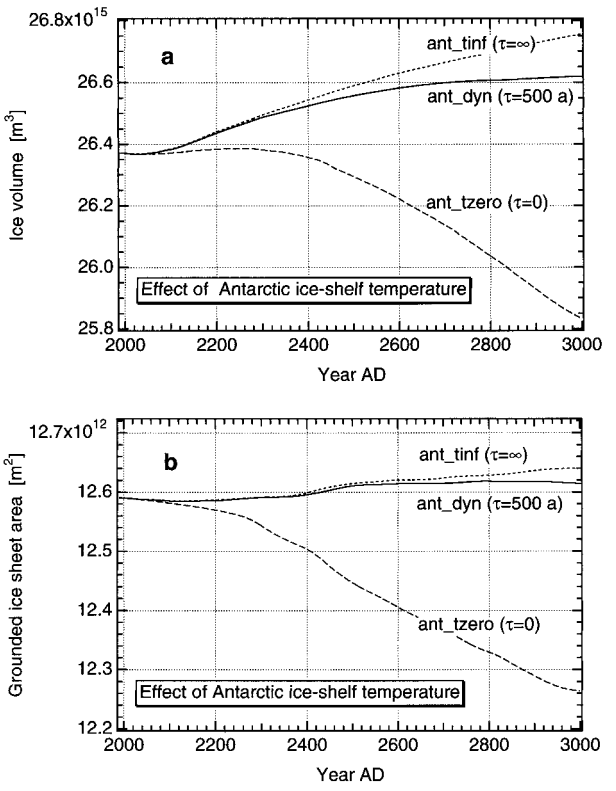

FIG. 13. Evolution of Antarctic ice volume (a) and grounded ice sheet area (b) in a series of experiments testing the effect of ice shelf temperature on grounding-line migration (ant_tinf, the effective ice shelf deformation temperature is fixed throughout the experiment; ant_tzero, the ice shelf temperature follows the surface perturbation instantaneously; ant_dyn, the characteristic timescale for ice shelf temperature change is 500 yr).

taneously to the applied surface warming (ant_tzero, $\tau^* = 0$) is shown in Fig. 13. It turns out that on the timescale considered in this paper (1000 yr), there is not so much difference between the runs with $\tau^* = \infty$ and $\tau^* = 500$ yr, but the assumption of an instantaneous warming of the shelf ($\tau^* = 0$) is found to lead to substantial grounding-line retreat. The ensuing reduction of ice volume (Fig. 13a) would in that case cause a global sea level rise of 1.35 m by the year 3000, which more than offsets the ice sheet growth resulting from the increased accumulation rates. The effect is evident right from the beginning of the integration. In the $\tau^* = 0$ run, grounding-line retreat compensates the growing trend due to the rising accumulation rates by 29% at 2050 A.D., by 41% at 2100 A.D., and becomes dominant after the year 2275 A.D. At that time, grounding-line retreat causes the Antarctic ice sheet to contribute positively to the global sea level stand. Clearly, the viscosity of the ice shelf constitutes a major control on grounding-line movements.

3) The effect of basal melting below the ice shelves

In all of the experiments discussed so far, basal melting beneath ice shelves was excluded from the forcing. This is simply because it is not well known how the oceanic circulation and heat exchange beneath ice shelves will react to a climatic warming and higher ocean temperatures. Factors such as summer ocean warming, length of the period with open water, thermohaline properties of the source water and the water circulation below the ice shelf are all expected to play a role, but a clear relation between temperature change and basal melting rates has not been established. Recent studies indicate that basal melt rates of up to 10 m yr^{-1} are well possible (Determann et al. 1991; Jacobs et al. 1996), though evidence has also been found for large areas of basal accretion below the Filchner-Ronne ice shelf (Oerter et al. 1992). Large melt rates thin the ice shelves, also near the grounding line, which should induce grounding-line retreat when transmitted to the grounded ice sheet. This transmission occurs in the model in two ways: steeper gradients across the grounding zone cause larger driving stresses, and higher deviatoric stress gradients across the grounding line contribute to the softening of the ice (Huybrechts 1990).

The effects of applying melt rates of between 1 and 10 m yr^{-1} are summarized in Fig. 14. These melt rates

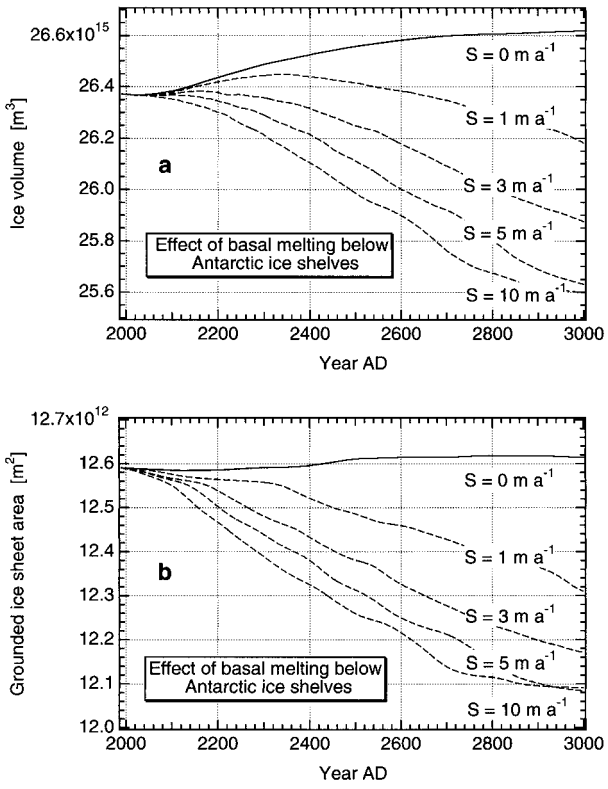

FIG. 14. Evolution of Antarctic ice volume (a) and grounded ice sheet area (b) in a series of experiments testing the effect of basal melting below the ice shelves. Here S is the basal melting rate in m yr^{-1}.

were not applied stepwise but were proportional to the mean annual temperature rise over Antarctica between 1990 and 2130 (Fig. 3). As can be judged from Fig. 14, melting below ice shelves is another very effective way to induce grounding-line retreat, which by the year 3000 eventually involves an area of between 2.2% (ant_s1, S = 1 m yr^{-1}) and 3.9% (ant_0, S = 10 m yr^{-1}) of the present ice sheet. Relative to the standard run without basal melting, the corresponding contributions to global sea level rise at 2500 A.D. are, respectively, +36 cm (S = 1 m yr^{-1}), +77 cm (S = 3 m yr^{-1}), +112 cm (S = 5 m yr^{-1}), and +144 cm (S = 10 m yr^{-1}), and thus generally of larger magnitude than the surface mass-balance effect of −46 cm obtained in the standard run (ant_dyn). Also here, the effect is evident from the beginning of the integration, but it lasts to between 2055 A.D. (S = 10 m yr^{-1}) and 2345 A.D. (S = 1 m yr^{-1}) before the effect of basal melting is large enough to counteract the surface mass-balance effect and cause Antarctic ice volume to decrease relative to the background evolution.

It is worth mentioning that the sensitivity of the Antarctic ice sheet to basal melting is not linear to the applied melt rate. From Fig. 14, it can be seen that the total retreat tends to a maximum for the highest melt rate. The reason is simply that the ice shelf thickness is eventually reduced to its minimum value of 10 m allowed for in the model. This minimum value is required in the finite-difference formulation of the model for numerical reasons (MacAyeal et al. 1996) but is physically equivalent to a nonexisting ice shelf. In terms of global sea level, the maximum rate of retreat in these experiments was found to be equivalent to about 25 cm century^{-1}. Though leading to substantial grounding-line retreat, we tend not to interpret this as an unstable collapse in the sense given to it in early papers by, for example, Mercer (1978). It is also realized, however, that the fast ice streams presently bordering the Ross ice shelf (but not elsewhere) are not explicitly modeled here and that the possibility of calving near the grounding line was not considered in case the ice shelves would disintegrate entirely. These factors could potentially speed up the response, though views on the possible role of ice streams and calving differ widely (e.g., Bentley 1997).

Figure 15 shows the resulting ice sheet geometries in those experiments that resulted in discernible changes of the ice sheet extent. The figure clearly makes the point that most of the change involves grounding-line retreat along the Ross Sea. For the middle scenario experiment with S = 10 m yr^{-1} (ant_s10) this occurs over a maximum distance of up to 500 km. Changes in the geometry of the east Antarctic ice sheet, on the other hand, are hardly distinguishable on the scale of the plots but involve a thickening of up to 100 m on the plateau and some grounding-line retreat along the most overdeepened outlet glaciers in the lower-right quadrant of the plotted ice sheet (in particular Totten, Ninis, and Mertz glaciers).

6. Conclusions

The results discussed in this paper indicate that on a multiple-century timescale the largest contribution to global sea level is to be expected from melting on the Greenland ice sheet. A likely estimate for the Greenland contribution to sea level rise is around 10 cm by the year 2100, with the possibility of a sea level rise of several meters by the year 3000 if greenhouse warming conditions are sustained after that. Even if greenhouse gas concentrations would stabilize by the early twenty-second century, Greenland meltdown is found to be irreversible for equivalent CO_2 concentrations more than twice the present value, reflecting the inertia of the system. On all timescales, ice dynamics and the height–mass-balance feedback were found to play a significant role to modify the mass-balance-only effect, whereas the present evolution of the ice sheet was small compared to the response to future warming.

The results for Antarctica provided a remarkable contrast. Here, the background trend would dominate the short-term (century) response and the ice-dynamic effect only becomes important on the longer term. Up to the end of the twenty-first century, the Antarctic ice

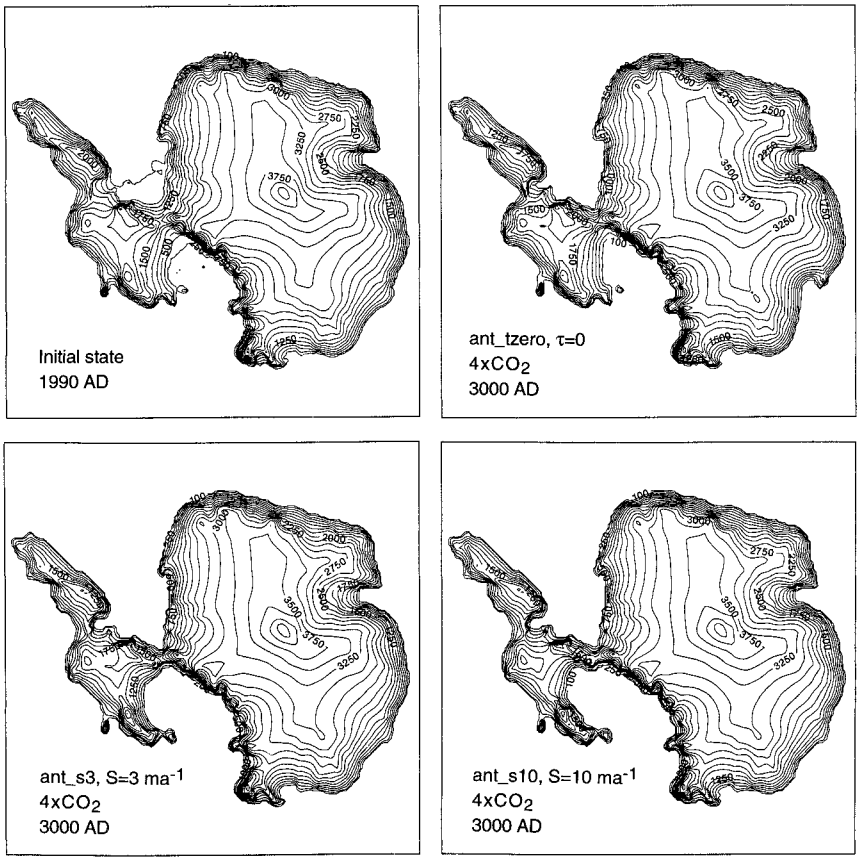

FIG. 15. Snapshots of Antarctic surface elevation for the experiments and times indicated in the lower-left corner and further detailed in Table 3 and the main text. These plots demonstrate that changes are mainly restricted to grounding-line recession in west Antarctica, whereas the east Antarctic ice sheet is hardly affected. Contour interval is 250 m; the lowest contour is close to the grounding line. All plots are for the middle scenario ($4 \times CO_2$).

sheet would roughly balance the sea level contribution of the Greenland ice sheet because increased accumulation rates would dominate over any melting. On the longer term, on the other hand, ice dynamics is found to contribute positively to sea level rise because of increased outflow into the ice shelves and grounding-line retreat along the west Antarctic ice sheet. Both effects were found to be quite sensitive to the basal melting rate below the ice shelves and the effective viscosity of the floating ice. Although basal melting rates of up to 10 m yr^{-1} show that substantial grounding-line retreat is certainly possible, the corresponding maximum rate of sea level rise of 25 cm $century^{-1}$ produced by the model does not, in our view, support the concept of a catastrophic collapse or strongly unstable behavior of the west Antarctic ice sheet.

Acknowledgments. Ph. Huybrechts would like to thank the Fund for Scientific Research–Flanders (FWO), the Belgian Impulse Programme on Global Change (Prime Minister's Office—Federal Office for Scientific, Technical, and Cultural Affairs), and the EU Framework IV project ''Climate change and sea level'' (ENV4-CT095-0124) for their support. Jan de Wolde obtained financial support from Rijkswaterstaat, RIKZ (project ''ZEESPIEG''), The Netherlands Geosciences Foundation (GOA), The Netherlands Organization for Scientific Research (NWO), and the EU Framework IV project ''Climate sensitivity of glacier mass-balance: The effect of topographic barriers'' (ENV4-CT095-0105). Much of this research was carried out at the Alfred-Wegener-Institut für Polar- und Meeresforschung in Bremerhaven, Germany. Generous access to their excellent working environment is gratefully acknowledged.

APPENDIX A

Description of the Ice Sheet Models

The Greenland and Antarctic ice sheet models basically solve prognostic equations for the conservation of ice volume and heat:

$$\frac{\partial H}{\partial t} = -\nabla \cdot (\bar{\mathbf{v}} H) + M \tag{A1}$$

$$\frac{\partial T_{\text{ice}}}{\partial t} = \frac{1}{\rho_{\text{ice}} c_p} \frac{\partial}{\partial z}\left(k_{\text{ice}} \frac{\partial T_{\text{ice}}}{\partial z}\right) - \mathbf{v}\nabla T_{\text{ice}} + \frac{2\dot{\varepsilon}\tau}{\rho_{\text{ice}} c_p} \tag{A2}$$

$$\frac{\partial T_{\text{rock}}}{\partial t} = \frac{k_{\text{rock}}}{\rho_{\text{rock}} c_{\text{rock}}} \frac{\partial^2 T_{\text{rock}}}{\partial z^2}, \tag{A3}$$

where H is the ice thickness, $\bar{\mathbf{v}}$ the depth-averaged horizontal velocity field, M the mass balance, and t the time. The thermodynamic equation [(A2)] accounts for vertical heat conduction, three-dimensional advection, and heat generation by internal deformation. Here, T is temperature, ρ_{ice} ice density [910 kg m^{-3}], $\mathbf{V}$ the three-dimensional ice velocity, $\dot{\varepsilon}$ and τ are the effective strain rate and effective deviatoric stress in the formulation of the strain heating, and k and c_p are temperature-dependent thermal conductivity and specific heat capacity of ice, respectively. In the bedrock [(A3)], only vertical heat conduction is considered, with $k_{\text{rock}} = 3.3$ W m^{-1} °C^{-1}, $\rho_{\text{rock}} = 3300$ kg m^{-3}, $c_{\text{rock}} = 1000$ J kg^{-1} °C^{-1}. The lower boundary condition is the geothermal heat flux of, respectively, 42 mW m^{-2} (Greenland) and 54.6 m W m^{-2} (Antarctica).

Grounded ice flow is assumed to result both from internal deformation and from sliding over the bed in those areas where the basal temperature is within 1°C from the pressure melting point. Ice deformation in the ice sheet domain is assumed to result from shearing in horizontal planes, and longitudinal deviatoric stresses are disregarded. A flow law of ''Glen type'' is used with exponent $n = 3$ and a rate factor $A(T_{\text{ice}})$, which depends on temperature and obeys an Arrhenius relation,

$$\dot{\varepsilon}_{ij} = mA(T_{\text{ice}})\tau^{n-1}\tau'_{ij}, \tag{A4}$$

where $\dot{\varepsilon}_{ij}$ are the strain rate components related to velocity gradients by definition, τ'_{ij} the stress deviators, and τ the effective stress defined in terms of all stress deviator components so that it is independent of the coordinate system. Here m is an enhancement factor that reflects the uncertainty in the rate factor and basically serves a tuning purpose.

Expressions for the horizontal velocity components result from substituting equations for the shear stress distribution $\tau(z)$ in the flow law and integrating the result with respect to the vertical. This yields

$$\boldsymbol{\tau}(z) = -\rho g(H + h - z)\nabla(H + h) \tag{A5}$$

$$\mathbf{v}(z) = -2(\rho g)^n [\nabla(H+h)\cdot\nabla(H+h)]\nabla(H+h) \times \int_h^z mA(T)(H + h - z)^n \, dz + \mathbf{v}(h) \tag{A6}$$

$$\bar{\mathbf{v}} H = \int_h^{H+h} \mathbf{v}(z) \, dz, \tag{A7}$$

where h is bed elevation.

Basal sliding increases with the third power of the basal shear stress τ:

$$\mathbf{v}(h) = -\frac{A_{sl}\boldsymbol{\tau}^n(h)}{Z}, \tag{A8}$$

where $A_{sl} = 1.8 \times 10^{-10}$ N^{-3} yr^{-1} m^8 and Z accounts for a reduced basal traction due to the pressure of subglacial water,

$$\begin{aligned} Z &= H && \text{if } h > H_{sl} \\ Z &= H + \rho_w(h - H_{sl})/\rho_i && \text{if } h < H_{sl}, \end{aligned} \tag{A9}$$

where ρ_w is sea water density [1028 kg m^{-3}] and H_{sl} is the sea level stand. Note that Eq. (A9) allows for increased sliding for ice grounded below sea level in deep outlet glaciers. A minimum value of 10^{-4} m is set on Z to avoid division by zero.

Both models are identical in their treatment of grounded ice but differ in their treatment of the ice margin. In the Greenland model, it is simply assumed that all ice that borders the coastline calves away as icebergs. As Antarctica has at present no appreciable surface melting and is surrounded by a floating ice shelf, migration of the grounding line is incorporated by coupling the inland-ice model with a dynamic flow model for ice shelves. In the ice shelf, the driving force is opposed by longitudinal gradients in normal deviatoric stresses and by lateral shearing induced by sidewalls and ice rises. That gives rise to the solution of a coupled set of elliptic partial differential equations to obtain the velocity field of the ice shelf, where it is no longer locally defined (MacAyeal et al. 1996):

$$\frac{\partial}{\partial x}\left[Hf\left(2\frac{\partial u}{\partial x} + \frac{\partial v}{\partial y}\right)\right] + \frac{1}{2}\frac{\partial}{\partial y}\left[Hf\left(\frac{\partial u}{\partial y} + \frac{\partial v}{\partial x}\right)\right] = \rho g H (mA(T))^{1/n}\frac{\partial(H + h)}{\partial x} \tag{A10a}$$

$$\frac{\partial}{\partial y}\left[Hf\left(2\frac{\partial v}{\partial y} + \frac{\partial u}{\partial x}\right)\right] + \frac{1}{2}\frac{\partial}{\partial x}\left[Hf\left(\frac{\partial u}{\partial y} + \frac{\partial v}{\partial x}\right)\right] = \rho g H [mA(T)]^{1/n}\frac{\partial(H + h)}{\partial y} \tag{A10b}$$

$$f = \left[\left(\frac{\partial u}{\partial x}\right)^2 + \left(\frac{\partial v}{\partial y}\right)^2 + \frac{1}{4}\left(\frac{\partial u}{\partial y} + \frac{\partial v}{\partial x}\right)^2 + \frac{\partial u}{\partial x}\frac{\partial v}{\partial y}\right]^{(1-n)/2n}, \tag{A10c}$$

where u and v are the horizontal velocity components, and f is a term that accounts for the nonlinearity of the flow law. The flow at the grounding line itself is treated as a transition zone between the floating and grounded flow regimes. Here, it is assumed that the ice sheet approximation is still valid but that all stress components contribute in the effective stress in the flow law. As demonstrated in Huybrechts (1990), this approach enables the grounding line to migrate in good agreement

with geological reconstructions on a glacial–interglacial timescale.

The rate factor, which is inversely proportional to the viscosity of the ice, depends primarily on temperature (Huybrechts and Oerlemans 1988). In the Greenland model, the rate factor furthermore allows for different mechanical characteristics of Holocene and ice-age ice, the latter of which is made to deform three times faster for the same stress and temperature conditions. The enhancement factor m [Eq. (A4)] was set at 4.5 for grounded ice and at 1 for ice shelves. Because the temperature field of ice shelves is strongly influenced by basal melting, which is poorly constrained, a full thermodynamic calculation in ice shelves was not made. Instead, it is assumed that the rate factor reflects vertically integrated conditions and that the effective deformation temperature T^* (defined as the arithmetic mean of the shelf's surface temperature and the freezing temperature of sea water) follows changes in surface temperature Δt by a time lag τ^*:

$$\frac{dT^*}{dt} = -\frac{1}{\tau^*}\left(T^* - \frac{\Delta T}{2}\right). \tag{A11}$$

From a simple one-dimensional heat flow model, it was derived that τ primarily depends on the ice thickness squared divided by the thermal diffusivity, whereas the magnitude of the mean ice shelf temperature change was primarily a function of the mass balance (advection). A value of 500 yr was adopted for τ^*, which is the characteristic timescale for heat conduction in a shelf with typical thickness of 500 m.

The horizontal resolution is 20 km for the Greenland model and 40 km for the Antarctic model. The Antarctic model has 11 layers in the vertical and the Greenland model has 26, with the closer spacing near to the bedrock where the shear concentrates. Rock temperatures are calculated down to a depth of 2.5 km, with a total of six points that are equally spaced 500 m apart. The finite-difference schemes are implicit in time, either alternatively in the x and y directions for the mass continuity equation, or only along the vertical for the thermodynamic equations, and were rigorously tested within the framework of the EISMINT Intercomparison Project (Huybrechts et al. 1996). All spatial differences are of second-order accuracy, including the upstream differences required to deal with the advection terms in the thermodynamic equation.

APPENDIX B

Description of the Isostasy Model

The bedrock adjustment model consists of an elastic plate (lithosphere) that overlies a viscous asthenosphere. This means that the isostatic compensation not only considers the load just above, but integrates the contributions from more remote locations, which gives rise to deviations from local isostasy. The downward deflection w created by a point load q for a floating elastic plate is a solution of

$$D\nabla^4 w = q - \rho_m g w, \tag{B1}$$

where D represents the flexural rigidity [1×10^{25} N m] and $\rho_m g w$ is the upward buoyancy force exerted on the deflected part of the lithosphere inside the asthenosphere, with ρ_m the mantle density (3300 kg m^{-3}). The deflection w at a normalized distance $x = r/L_r$ from the point load can be written as

$$w(x) = \frac{qL_r^2}{2\pi D} kei(x), \tag{B2}$$

with $kei(x)$ a Kelvin function of zero order, r the real distance from the load q, and L_r the so-called radius of relative stiffness [$L_r = (D/\rho_m g)^{1/4}$]. A point load will cause a depression within a distance of four times L_r ($L_r = 130$ km for a 115 km thick lithosphere). Beyond this distance, a small bulge appears. As lithosphere deflection is a linear process, the total deflection at each point is calculated as the sum of the contributions of all the neighboring points within a distance of about five to six times L_r (650–780 km). The loading takes into account contributions from both ice and ocean water.

The asthenosphere responds to changes in the loading in a damped fashion with a characteristic timescale Θ of 3000 yr:

$$\frac{\partial h}{\partial t} = \frac{-1}{\Theta}(h - h_0 + w), \tag{B3}$$

where h_0 is the undisturbed bed topography when the load is removed and isostatic rebound is complete. The latter treatment to accommodate for the viscous response of the asthenosphere is preferred over the diffusion approach employed in previous versions of the model, which was characterized by an unrealistic relation between the size of the load and the relaxation time (Le Meur and Huybrechts 1996).

APPENDIX C

Description of the Mass-Balance Model

The mass-balance model has been updated with respect to previous studies and is therefore described in more detail. Central to the various mass-balance components are parameterizations for surface temperature derived from climatic data. For the Antarctic ice sheet, the following relations were adopted:

$$\text{TMA} = 34.46 + \gamma_a H_{\text{sur}} - 0.68775\Phi + \Delta T \tag{C1}$$

$$\text{TMS} = 16.81 + \gamma_s H_{\text{sur}} - 0.27937\Phi + \Delta T \tag{C2}$$

$$T_{\text{monthly}} = \text{TMA} - (\text{TMS} - \text{TMA})\cos(2\pi t/A). \tag{C3}$$

And for the Greenland ice sheet,

$$\text{TMA} = 49.13 + \gamma_g H_{\text{sur}} - 0.7576\Phi + \Delta T \quad \text{if } H_{\text{sur}} \geq H_{\text{inv}} \tag{C4}$$

$$\text{TMA} = 49.13 + \gamma_g H_{\text{inv}} - 0.7576\Phi + \Delta T \quad \text{if } H_{\text{sur}} < H_{\text{inv}} \tag{C5}$$

$$H_{\text{inv}} = 20(\Phi - 65) \tag{C6}$$

$$\text{TMS} = 30.78 + \gamma_z H_{\text{sur}} - 0.3262\Phi + \Delta T \tag{C7}$$

$$T_{\text{monthly}} = \text{TMA} - (\text{TMS} - \text{TMA}) \cos(2\pi t/A), \tag{C8}$$

where H_{sur} is surface elevation (m); Φ geographical latitude (in ° and positive in both hemispheres); ΔT the applied temperature change as a function of geographical position and time produced by the climate model; TMA the mean annual temperature, TMS summer temperature, and T_{monthly} mean monthly temperature, respectively (°C); and $\gamma_a = -0.005\,102$ for $H_{\text{sur}} < 1500$ m and $\gamma_a = -0.014\,285$ for $H_{\text{sur}} > 1500$ m, $\gamma_s = -0.006\,92$, $\gamma_g = -0.007\,992$, $\gamma_z = -0.006\,277$ are atmospheric lapse rates (°C m^{-1}). Here A is a period of 1 yr and H_{inv} (m) the altitude in Greenland, below which a temperature inversion is usually observed.

The precipitation model makes a distinction between snowfall and rainfall. The snow accumulation rate is defined as the fraction of precipitation that falls at surface temperatures below 2°C:

$$\text{Acc} = (1 - R) \times \text{Prec}, \tag{C9}$$

where R is the time fraction of the year during which temperatures are above 2°C, and Prec and Acc (both expressed in m yr^{-1} of ice equivalent) are the precipitation and the accumulation rate, respectively. The fraction R is calculated with a statistic that is normally distributed and centered on the curve of the mean daily temperature with a standard deviation σ of 5°C, accounting for random temperature fluctuations and the daily cycle:

$$R = \frac{1}{\sigma\sqrt{2\pi}} \int_0^A \left\{ \int_2^{T_{\text{monthly}}+2.5\sigma} \exp\left[\frac{-(T - T_{\text{monthly}})^2}{2\sigma^2}\right] dT \right\} dt. \tag{C10}$$

Precipitation in different climates are calculated as ratios of the presently observed precipitation intensities, as digitized from maps (Ohmura and Reeh 1991; Huybrechts and Oerlemans 1990). For the Antarctic, the following procedure is adopted:

$$T_{\text{inv}} = 0.67 T_{\text{sur}} + 88.9 \tag{C11}$$

$$\text{Prec}[T_{\text{inv}}(t)] = \text{Prec}[T_{\text{inv}}(\text{present})] \times \exp\left\{22.47\left[\frac{T_0}{T_{\text{inv}}(\text{present})} - \frac{T_0}{T_{\text{inv}}(t)}\right]\right\} \times \left\{\frac{T_{\text{inv}}(\text{present})}{T_{\text{inv}}(t)}\right\}^2, \tag{C12}$$

where T_{inv} (K) is the mean annual temperature above the surface inversion layer, T_{sur} (K) the mean annual surface temperature, Prec the precipitation rate (in m yr^{-1} of ice equivalent), and $T_0 = 273.16$ K. This treatment is based on the observation that the accumulation rate over Antarctica appears to be well correlated with the water vapor pressure gradient relative to the condensation temperature above the surface inversion layer, as established on a glacial–interglacial timescale (Robin 1977; Lorius et al. 1985). For surface temperatures prevailing over Antarctica, resulting precipitation rates are typically doubled for a temperature rise of 10°C.

Above the Greenland ice sheet a more simple parameterization is employed that is however inspired by the same physical principle. Here, the presently observed precipitation rate is prescribed to vary by a sensitivity $(1 + s)$ for every degree of temperature change ΔT:

$$\text{Prec}(\Delta T) = \text{Prec}(0)(1 + s)^{\Delta T} \tag{C13}$$

$$s = \begin{cases} 0.05 & \Delta T \geq 0°\text{C} \\ 0.05 - 0.005\Delta T & -10°\text{C} \leq \Delta T \leq 0°\text{C} \\ 0.10 & \Delta T \leq -10°\text{C}, \end{cases} \tag{C14}$$

where Prec(0) and Prec(ΔT) are precipitation rates [m yr^{-1}] for present conditions and for a temperature perturbation ΔT, respectively. The temperature dependence of the factor $(1 + s)$ is a refinement with respect to previous studies. It combines the change in precipitation rate per degree Celsius of 5.33% found by Clausen et al. (1988) from shallow ice cores spanning the late Holocene with the 8%–9% value derived by Dahl-Jensen et al. (1993) for the upper 2321 m of the GRIP core. The relation adopted in (C13)–(C14) is also in better agreement with accumulation studies conducted on the Greenland Ice Sheet Project 2 core (Kapsner et al. 1994). For a temperature rise of 5°C, precipitation rates increase by 27.6%, and for a cooling of 10°C, they are reduced by 61.4%.

Following procedures successfully adopted previously (Huybrechts et al. 1991), the amount of melting is conveniently obtained from a degree-day model. The total amount of positive degree days (PDD) is obtained as

$$\text{PDD} = \frac{1}{\sigma(2\pi)^{1/2}} \int_0^A \times \left\{ \int_0^{T_{\text{monthly}}+2.5\sigma} T \exp\left[\frac{-(T - T_{\text{monthly}})^2}{2\sigma^2}\right] dT \right\} dt, \tag{C15}$$

where σ is also taken as 5°C (Reeh 1991). The annual number of positive degree days represents a melt potential, which is subsequently used to melt snow and (superimposed) ice with degree-day factors of 0.003 m (PDD)$^{-1}$ and of 0.008 m (PDD)$^{-1}$ of ice equivalent, respectively.

The liquid water produced by the model (meltwater and rain) will at first refreeze in the snowpack and produce superimposed ice. Refreezing of meltwater is an important process on Greenland and in the Canadian Arctic and can be expected to significantly retard runoff on Antarctica when melting starts in a warmer climate. In the model, the amount of refreezing depends on the cold content of the upper ice sheet layers, which puts an upper limit on the production of superimposed ice [m yr^{-1}]:

$$\mathrm{Ice}_{\mathrm{superimposed}} = \frac{(T_m - T_{\mathrm{air}})_{\mathrm{year}} \times 2m \times c_p}{L}. \quad \text{(C16)}$$

The maximum amount of superimposed ice is equivalent to the latent heat released to raise the temperature of the uppermost 2 m of the ice sheet surface from the mean annual temperature to the melting point T_m (L: latent heat of fusion, 3.35×10^5 J kg^{-1}; c_p: specific heat capacity of ice, 2009 J kg^{-1} °C^{-1}). This value gives a good fit to a number of detailed measurements reported by Ambach (1963) (cf. Oerlemans 1991). Once this upper limit is reached, any additional snowmelt and/or rainfall is assumed to run off. In this treatment, the yearly mass balance thus becomes negative when all of the yearly snowfall and superimposed ice, if any, has melted away. Because of their very low surface slopes, the model further assumes that the meltwater produced on the surface of the Antarctic ice shelves does not run off but refreezes in situ. The mass-balance treatment over Antarctica and Greenland is the same for warmer as well as for colder climates than today. The main effect of the modifications of the mass-balance model with respect to earlier versions (Huybrechts and Oerlemans 1990; Huybrechts et al. 1991) is to yield a higher sensitivity in warmer climates, which is also more in accordance with energy-balance calculations (van de Wal 1996).

APPENDIX D

Description of the Climate and Ocean Model

The zonal mean energy-balance climate model has a vertical and latitudinal resolution and resolves the seasonal cycle. The ocean model consists of three zonally averaged ocean basins, representing the Atlantic, Pacific, and Indian Oceans, which are connected by a circumpolar ocean basin, representing the Southern Ocean. The model has a prescribed ocean circulation and includes several parameterizations of ocean heat mixing due to unresolved eddies. The ocean temperature fields are affected by ocean heat mixing and by advection by the mean flow. At the surface, the oceans exchange radiative and turbulent energy with the atmosphere:

$$\frac{\partial T_{\mathrm{oce}}}{\partial t} + \frac{1}{rf\cos\varphi}\frac{\partial (ufT_{\mathrm{oce}}\cos\varphi)}{\partial \varphi} + \frac{\partial (wT_{\mathrm{oce}})}{\partial z} = \frac{1}{r^2 f\cos\varphi}\frac{\partial}{\partial \varphi}\left(fD_h\cos\varphi\frac{\partial T_{\mathrm{oce}}}{\partial \varphi}\right) + \frac{\partial}{\partial z}\left(D_v\frac{\partial T_{\mathrm{oce}}}{\partial z}\right) + \frac{\Delta L_{\mathrm{oce}} + \Delta S_{\mathrm{oce}} - \mathrm{SH} - \mathrm{LH}}{\rho_w c_w d_s}, \quad \text{(D1)}$$

where r is the earth's radius and ϕ the latitude; T_{oce} the ocean temperature; f the fractional ocean width for each basin separately ($f_{\mathrm{atl}} + f_{\mathrm{pac}} + f_{\mathrm{ind}} = 1 - f_{\mathrm{land}}$); u the meridional velocity, w the vertical velocity; z the vertical coordinate; D_h and D_v the horizontal and vertical diffusion processes, respectively; SH and LH the turbulent sensible and latent heat fluxes at the surface, respectively; ΔL_{oce} and ΔS_{oce} the net longwave and shortwave radiative fluxes at the surface, respectively; ρ_w the density of sea water; c_w the specific heat capacity of sea water; and d_s the thickness of the uppermost ocean layer (75 m). The last term on the right-hand side, which represents the surface energy exchange with the atmosphere, applies to the surface layer only. The ocean model is identical to that described by de Wolde et al. (1995), but includes a representation of sea ice. Since horizontal variations in sea ice extent are assumed to affect the surface energy budget most by means of the albedo, these are calculated as described by Bintanja (1997). Sea ice forms with a specified thickness of 1.5 m and the formation is determined by thermodynamics only.

In the climate model, which is identical to that used by Bintanja (1997), the atmosphere is represented by a vertically and zonally averaged layer of air. Fluxes of shortwave and longwave radiation at the top and bottom of the atmospheric layer are calculated by means of parameterizations in terms of the solar zenith angle, cloud amount, cloud optical depth, water vapor content, and the amount of ozone and carbon dioxide. The absorption and reflection of solar radiation at the earth's surface are determined by the surface albedo of land, ocean water, and sea ice. The radiative effects of aerosols are not considered. Turbulent fluxes at the surface are determined by bulk formulas. The model is driven by the daily mean incoming shortwave radiation at the top of the atmosphere. The meridional heat transport is modeled as a diffusive process in terms of the atmospheric surface temperature. The meridional distribution of the atmospheric diffusion coefficient is taken from Harvey (1988). The ''infinite wind'' case is adopted in the climate model to calculate the zonal heat transport between land and ocean. This means that one effective atmospheric layer is assumed that overlies the land as well as the ocean part of a latitudinal band. The zonal mean surface air temperature (T_{atm}) in the model is thus calculated according to the following equation:

$$\frac{\partial T_{\text{atm}}}{\partial t} = \frac{1}{r^2 \cos\varphi}\frac{\partial}{\partial \varphi}\left(D_a \cos\varphi \frac{\partial T_{\text{atm}}}{\partial \varphi}\right) + \frac{\Delta L_{\text{atm}} + \Delta S_{\text{atm}} + \text{SH} + \text{LH}}{R_a}, \quad \text{(D2)}$$

where r is the earth's radius and ϕ the latitude; D_{atm} the atmospheric diffusion coefficient; SH and LH are the sensible and latent heat fluxes at the surface, respectively; ΔL_{atm} and ΔS_{atm} the divergence of the longwave and shortwave radiation, respectively; and R_{atm} is the atmospheric thermal inertia. The last term on the right-hand side represents the area-weighted zonal mean values of the individual atmosphere–surface energy fluxes above land and above the oceans.

The climate model was calibrated against the seasonal cycle of present-day observations of surface air temperature, ocean temperatures, and snow and sea ice cover. The climate sensitivity of the model (defined as the equilibrium global mean surface air temperature increase due to a doubling of the CO_2 concentration) is 2.2°C, close to the best estimate of 2.5°C based on observational evidence, on general circulation model studies and on sensitivity analyses (Kattenberg et al. 1996).

REFERENCES

Ambach, W., 1963: Untersuchungen zum Energieumsatz in der Ablationszone des Grönlandischen Inlandeises (Camp IV-EGIG, 69°40′05″N, 49°37′58″W). *Medd. Grønl.,* **174**(4), 311 pp.

Bintanja, R., 1997: Sensitivity experiments performed with an energy balance atmosphere model coupled to an advection-diffusion ocean model. *Theor. Appl. Climatol.,* **56,** 1–24.

Bentley, C. R., 1997: Rapid sea-level rise soon from West Antarctic ice sheet collapse? *Science,* **275,** 1077–1078.

Budd, W. F., D. Jenssen, E. Mavrakis, and B. Coutts, 1994: Modelling the Antarctic Ice Sheet changes through time. *Ann. Glaciol.,* **20,** 291–297.

Clausen, H. B., N. S. Gundestrup, S. J. Johnsen, R. Bindschadler, and J. Zwally, 1988: Glaciological investigations in the Crete area, Central Greenland. A search for a new drilling site. *Ann. Glaciol.,* **10,** 10–15.

Dahl-Jensen, D., S. J. Johnson, C. U. Hammer, H. B. Clausen, and J. Jouzel, 1993: Past accumulation rates derived from observed annual layers in the GRIP ice core from Summit, Central Greenland. *Ice in the Climate System,* W. R. Peltier, Ed., NATO ASI Series, Vol. I 12, Springer-Verlag, 517–532.

Dansgaard, W., and Coauthors, 1993: Evidence for general instability of past climate from a 250-yr ice-core record. *Nature,* **364,** 218–220.

Denton G. H., M. L. Prentice, and L. H. Burckle, 1990: Cainozoic history of the Antarctic ice sheet. *Geology of Antarctica,* R. Tingey, Ed., Oxford University Press, 366–433.

Determann, J., K. Grosfeld, and B. Ritter, 1991: Melting rates at the bottom of Filchner–Ronne ice shelf, Antarctica, from short-term mass-balance studies. *Polarforschung,* **60** (1), 25–32.

de Wolde, J. R., 1996: A zonally averaged climate model for thermal expansion: Comparison with GCM's and a 1D upwelling-diffusion model. IMAU Internal Rep. R96-13, 25 pp. [Available from Jan de Wolde, Institut voor Marienen Atmosferisch Onderzoek, Universiteit Utrecht, Princetonplein 5, NL-3584 CC Utrecht, Netherlands.]

——, R. Bintanja, and J. Oerlemans, 1995: On thermal expansion over the last hundred years. *J. Climate,* **8,** 2881–2891.

——, P. Huybrechts, J. Oerlemans, and R. S. W. van de Wal, 1997: Projections of global mean sea level rise calculated with a 2D energy-balance climate model and dynamic ice sheet models. *Tellus,* **49A,** 486–502.

Drewry, D. J., and E. M. Morris, 1992: The response of large ice sheets to climatic change. *Philos. Trans. Roy. Soc. London,* **338B,** 235–242.

Harvey, L. D. D., 1988: A semianalytic energy balance climate model with explicit sea ice and snow physics. *J. Climate,* **1,** 1065–1085.

Hasselmann, K., R. Sausen, E. Maier-Reimer, and R. Voss, 1993: On the cold start problem in transient simulations with coupled atmosphere–ocean models. *Climate Dyn.,* **9,** 53–61.

Houghton, J. T., L. G. Meira Filho, B. A. Callander, N. Harris, A. Kattenberg, and K. Maskell, Eds., 1996: *Climate Change 1995.* Cambridge University Press, 572 pp.

Huybrechts, P., 1990: A 3-D model for the Antarctic Ice Sheet: A sensitivity study on the glacial–interglacial contrast. *Climate Dyn.,* **5,** 79–92.

——, 1992: The Antarctic Ice Sheet and environmental change: A three-dimensional modeling study. *Ber. Polarforschung,* **99,** 241 pp.

——, 1994a: Formation and disintegration of the Antarctic ice sheet. *Ann. Glaciol.,* **20,** 336–340.

——, 1994b: The present evolution of the Greenland ice sheet: An assessment by modelling. *Global Planet. Change,* **9,** 39–51.

——, 1996: Basal temperature conditions of the Greenland ice sheet during the glacial cycles. *Ann. Glaciol.,* **23,** 226–236.

——, and J. Oerlemans, 1988: Evolution of the East Antarctic ice sheet: A numerical study of thermo-mechanical response patterns with changing climate. *Ann. Glaciol.,* **11,** 52–59.

——, and ——, 1990: Response of the Antarctic Ice Sheet to future greenhouse warming. *Climate Dyn.,* **5,** 93–102.

——, A. Letreguilly, and N. Reeh, 1991: The Greenland ice sheet and greenhouse warming. *Paleogeogr. Paleoclim. Paleoecol.,* **89,** 399–412.

——, and Coauthors, 1996: The EISMINT benchmarks for testing ice-sheet models. *Ann. Glaciol.,* **23,** 1–12.

Imbrie, J., and Coauthors, 1984: The orbital theory of Pleistocene climate: Support from a revised chronology of the marine $\delta^{18}O$ record. *Milankovitch and Climate,* A. Berger, et al., Eds., NATO ASI Series C126, D. Reidel, 269–305.

Jacobs, S. S., H. H. Hellmer, and A. Jenkins, 1996: Antarctic ice sheet melting in the Southeast Pacific. *Geophys. Res. Lett.,* **23** (9), 957–960.

Jouzel, J., and Coauthors, 1993: Extending the Vostok ice-core record of palaeoclimate to the penultimate glacial period. *Nature,* **364,** 407–412.

Kapsner, W. R., R. B. Alley, C. A. Shuman, S. Anandakrishnan, and P. M. Grootes, 1994: Dominant influence of atmospheric circulation on snow accumulation in Greenland over the past 18,000 years. *Nature,* **373,** 52–54.

Kattenberg, A., and Coauthors, 1996: Climate models—Projections of future climate. *Climate Change 1995,* J. T. Houghton, et al., Eds., Cambridge University Press, 285–357.

Kim, K.-Y., and T. J. Crowley, 1994: Modelling the climate effect of unrestricted greenhouse emissions over the next 100 000 years. *Geophys. Res. Lett.,* **21** (8), 681–684.

Le Meur, E., and P. Huybrechts, 1996: A comparison of different ways of dealing with isostasy: Examples from modeling the Antarctic ice sheet during the last glacial cycle. *Ann. Glaciol.,* **23,** 309–317.

Letreguilly, A., P. Huybrechts, and N. Reeh, 1991: Steady-state characteristics of the Greenland ice sheet under different climates. *J. Glaciol.,* **37** (125), 149–157.

Lorius, C., J. Jouzel, C. Ritz, L. Merlivat, N. J. Barkov, Y. S. Korotkevich, and V. M. Kotlyakov, 1985: A 150 000-year climatic record from Antarctic ice. *Nature,* **316,** 591–596.

Loutre, M.-F., 1995: Greenland ice sheet over the next 5000 years. *Geophys. Res. Lett.,* **22** (7), 783–786.

MacAyeal, D. R., V. Rommelaere, P. Huybrechts, C. L. Hulbe, J.

Determann, and C. Ritz, 1996: An ice-shelf model test based on the Ross ice shelf. *Ann. Glaciol.,* **23,** 46–51.

Manabe, S., and R. J. Stouffer, 1993: Century-scale effects of increased atmospheric CO_2 on the ocean–atmosphere system. *Nature,* **364,** 215–218.

Mercer, J. H., 1978: West Antarctic ice sheet and CO_2 greenhouse effect: A threat of disaster. *Nature,* **271,** 321–325

Nakada, M., and K. Lambeck, 1988: The melting history of the late Pleistocene Antarctic ice sheet. *Nature,* **333,** 36–40.

Oerlemans, J., 1982: Response of the Antarctic ice sheet to a climatic warming: A model study. *J. Climatol.,* **2,** 1–11.

——, 1991: The mass balance of the Greenland ice sheet: Sensitivity to climate change as revealed by energy-balance modelling. *The Holocene,* **1** (1), 40–49.

Oerter, H., J. Kipfstuhl, J. Determann, H. Miller, D. Wagenbach, A. Minikin, and W. Graf, 1992: Evidence for basal marine ice in the Filchner-Ronne ice shelf. *Nature,* **358,** 399–401.

Ohmura, A., and N. Reeh, 1991: New precipitation and accumulation maps for Greenland. *J. Glaciol.,* **37,** 140–148.

——, M. Wild, and L. Bengtsson, 1996: A possible change in mass balance of Greenland and Antarctic ice sheets in the coming century. *J. Climate,* **9,** 2124–2135.

Raper, S. C. B., T. M. L. Wigley, and R. A. Warrick, 1996: Global sea level rise: Past and future. *Rising Sea Level and Subsiding Coastal Area,* J. D. Milliman, Ed., Kluwer Academic, 384 pp.

Reeh, N., 1991: Parameterization of melt rate and surface temperature on the Greenland Ice Sheet. *Polarforschung,* **59,** 113–128.

Robin, G. de Q., 1977: Ice cores and climatic change. *Philos. Trans. Roy. Soc. London,* **280,** 143–168.

Santer, B. D., K. E. Taylor, T. M. L. Wigley, J. E. Penner, P. D. Jones, and U. Cubasch, 1995: Towards the detection and attribution of an anthropogenic effect on climate. *Climate Dyn.,* **12,** 77–100.

——, and Coauthors, 1996: A search for human influences on the thermal structure of the atmosphere. *Nature,* **382,** 39–46.

Tushingham, A. M., and W. R. Peltier, 1991: Ice-3G: A new global model of late pleistocene deglaciation based upon geophysical predictions of post-glacial relative sea level change. *J. Geophys. Res.,* **96** (B3), 4497–4523.

van de Wal, R. S. W., 1996: Mass balance modelling of the Greenland ice sheet: A comparison of an energy balance and a degree-day model. *Ann. Glaciol.,* **23,** 36–45.

——, and J. Oerlemans, 1997: Modelling the short term response of the Greenland ice sheet to global warming. *Climate Dyn.,* **13,** 733–744.

van Tatenhove, F. G. M., J. J. M. van der Meer, and P. Huybrechts, 1995: Glacial geological/geomorphological research in west Greenland used to test an ice-sheet model. *Quat. Res.,* **44,** 317–327.

Verbitsky, M., and R. J. Oglesby, 1995: The CO_2-induced thickening/thinning of the Greenland and Antarctic ice sheets as simulated by a GCM (CCM1) and an ice-sheet model. *Climate Dyn.,* **11,** 247–253.

Walker, J. C. G., and J. F. Kasting, 1992: Effects of fuel and forest conservation on future levels of atmospheric carbon dioxide. *Global Planet. Change,* **97,** 151–189.

Warrick, R. A., and Coauthors, 1996: Changes in sea level. *Climate Change 1995,* J. T. Houghton et al., Eds., Cambridge University Press, 359–405.

Wigley, T. M. L., 1995: Global-mean temperature and sea level consequences of greenhouse gas concentration stabilization. *Geophys. Res. Lett.,* **22** (1), 45–48.